



UNIVERSITY OF LEEDS

This is a repository copy of *Mass-Transport Complexes as Markers of Deep-Water Fold-and-Thrust Belt Evolution: Insights from the Southern Magdalena Fan, Offshore Colombia*.

White Rose Research Online URL for this paper:
<http://eprints.whiterose.ac.uk/100691/>

Version: Accepted Version

Article:

Ortiz-Karpf, A, Hodgson, DM orcid.org/0000-0003-3711-635X, Jackson, CA-L et al. (1 more author) (2018) Mass-Transport Complexes as Markers of Deep-Water Fold-and-Thrust Belt Evolution: Insights from the Southern Magdalena Fan, Offshore Colombia. *Basin Research*, 30 (S1). pp. 65-88. ISSN 0950-091X

<https://doi.org/10.1111/bre.12208>

© 2016 The Authors. This is the peer reviewed version of the following article: Ortiz-Karpf, A, Hodgson, DM, Jackson, CA-L and McCaffrey, WD, (2016) Mass-Transport Complexes as Markers of Deep-Water Fold-and-Thrust Belt Evolution: Insights from the Southern Magdalena Fan, Offshore Colombia. *Basin Research*, 30: 65–88, which has been published in final form at <http://doi.org/10.1111/bre.12208>. This article may be used for non-commercial purposes in accordance with Wiley Terms and Conditions for Self-Archiving.

Reuse

Unless indicated otherwise, fulltext items are protected by copyright with all rights reserved. The copyright exception in section 29 of the Copyright, Designs and Patents Act 1988 allows the making of a single copy solely for the purpose of non-commercial research or private study within the limits of fair dealing. The publisher or other rights-holder may allow further reproduction and re-use of this version - refer to the White Rose Research Online record for this item. Where records identify the publisher as the copyright holder, users can verify any specific terms of use on the publisher's website.

Takedown

If you consider content in White Rose Research Online to be in breach of UK law, please notify us by emailing eprints@whiterose.ac.uk including the URL of the record and the reason for the withdrawal request.



eprints@whiterose.ac.uk
<https://eprints.whiterose.ac.uk/>

**Mass-Transport Complexes as Markers of Deep-Water Fold-and-Thrust Belt Evolution:
Insights from the Southern Magdalena Fan, Offshore Colombia**

Running title: MTCs as markers of deep-water fold belt evolution

Andrea Ortiz-Karpf

School of Earth and Environment, University of Leeds, Leeds LS2 9JT, United
Kingdom

Tel: +44(0)7450313365

eealok@leeds.ac.uk

David M. Hodgson

School of Earth and Environment, University of Leeds, Leeds LS2 9JT, United
Kingdom

Tel: +44(0)113 343 0236

D.Hodgson@leeds.ac.uk

Christopher A.-L. Jackson

Basins Research Group (BRG), Department of Earth Science and Engineering, Imperial
College, Prince Consort Road, London, SW7 2BP, UK

Tel: +44(0)207 59 47450

c.jackson@imperial.ac.uk

William D. McCaffrey

School of Earth and Environment, University of Leeds, Leeds LS2 9JT, United
Kingdom

Tel: +44(0)011334-36625

W.D.McCaffrey@leeds.ac.uk

May 2016

Abstract

Mass-wasting is an important process in the degradation of deep-water fold-and-thrust belts. However, the relationship between mass-transport complex (MTC) emplacement and the timing and spatial progression of contractional deformation of the seabed have not been extensively studied. This study uses high-quality, 3D seismic reflection data from the southern Magdalena Fan, offshore Colombia to investigate how the growth of a deep-water fold-and-thrust belt (the southern Sinú Fold Belt) is recorded in the source, distribution and size of MTCs. More than nine distinct, but coalesced MTCs overlie a major composite basal erosion surface. This surface formed by multiple syn- and post-tectonic mass-wasting events and is thus highly diachronous, thereby recording a protracted period of tectonism, seascape degradation and associated sedimentation. The size and source location of these MTCs changed through time: the oldest 'detached' MTCs are relatively small (over 9-100 km² in area) and sourced from the flanks of growing anticlines, whereas the younger 'shelf-attached' MTCs are considerably larger (more than 200-300 km²), are sourced from the shelf, and post-date the main phase of active folding and thrusting. Changes in the source, distribution and size of MTCs are tied to the sequential nucleation, amplification and along-strike propagation of individual structures, showing that MTCs can be used to constrain the timing and style of contractional deformation, and seascape evolution in time and space.

Key Words

1. Tectonics and sedimentation
2. Deep-water fold-and-thrust belt
3. Mass-transport complexes (MTC)
4. Magdalena Fan
5. Offshore Colombia
6. Caribbean
7. Subduction-related basins

1. Introduction

Mass-transport complexes (MTCs) were originally defined using seismic reflection data (Weimer, 1990) and they include a spectrum of deposit types (slides, slumps and debrites; e.g. Dott, 1963; Nemec, 1990; Shanmugam et al., 1994; Moscardelli et al., 2006; Moscardelli & Wood, 2008; Manica, 2012). Moscardelli & Wood (2008) define relatively small gravitational failures caused by local oversteepening of the submarine slope as *detached*

MTCs; these are typically thin (<100 m) and may cover only a few tens of square kilometres. Large failures of the shelf edge, which may be caused by earthquakes, gas-hydrate dissolution, increased sediment supply or sea-level change (e.g. Manley & Flood, 1988; Beaubouef & Friedmann, 2000; Maslin et al., 2004; Frey-Martinez et al., 2005; Grozic, 2010; Masson et al., 2010) are termed *shelf-attached MTCs* (Moscardelli & Wood, 2008). Shelf-attached MTCs can reach thousands of square kilometres in area and be hundreds of metres thick (Moscardelli & Wood, 2008; 2015).

Commonly, submarine fold-and-thrust belts in both active and passive tectonic margins are degraded by mass-wasting events and are thus flanked by MTCs (e.g. Heniö & Davies, 2006; Clark & Cartwright, 2009; 2012; Vinnels et al., 2010; Romero-Otero, 2010; Geersen et al., 2011; Alfaro & Holz, 2014; Idárraga-García & Vargas 2014; Vargas & Idárraga-García 2014; Festa et al., 2015, Yarbuh & Contreras, 2015). Previous studies focused on salt-or-shale-based passive margins prone to thin-skinned deformation have considered the relationship between MTC emplacement and structural evolution. For example, Heniö & Davies (2006) use 3D seismic data from the Niger Delta to examine the three-dimensional degradation of compressional folds created by gravity tectonics. Clark and Cartwright (2012) analysed the distribution and architecture of channel-levee complexes and MTCs within a growth package in a fold in the deep-water fold-and-thrust-belt in the Western Niger Delta in order to reconstruct the three-dimensional, sequential development of structural relief.

On tectonically-active continental margins, recurrent mass-wasting is commonly caused by seabed oversteepening due to structurally induced seabed deformation and/or by seismic activity (e.g. Moore et al., 1976; Torelli et al., 1997; Goldfinger et al., 2000; Frey-Martinez et al., 2005; 2006; Minisini et al., 2007; Lamarche, 2008; Cattaneo et al., 2010; Dan et al., 2010; Romero-Otero et al., 2010; Geersen et al., 2011; Alfaro & Holz, 2014; Festa et al., 2015; Perez et al., 2016). Several studies on active margins have investigated the mechanisms for slope failure and provide detailed descriptions of the deposits resulting from fold degradation (e.g. Trincardi & Argnani, 1990; Moscardelli & Wood., 2008; 2015; Rogers & Goodbred, 2010; Romero-Otero, 2010; Alfaro & Holz, 2014; Idárraga-García & Vargas 2014; Vargas & Idárraga-García 2014). However, few relate MTC emplacement to the tectono-stratigraphic evolution of the basin margin. For example, Geersen et al. (2011) relate a series of large-scale slope collapses with the regional tectonic history and present a two-dimensional model for the evolution of mass-failures offshore Chile. Festa et al. (2015) present a detailed outcrop study that investigates the relationship between the distribution of MTCs and the tectonostratigraphic evolution of the northern Apennines. Pérez et al. (2016) document variations in the dimensions, and vertical and spatial distribution of MTCs in several basins with different deformation styles along the Scotia-Antarctica plate margin, and

relate them to the regional tectonic evolution. However, there is still a paucity of detailed, three-dimensional analyses that link the timing, location and character of MTCs with the growth of individual structures within the developing deep-water fold-and-thrust belts. Furthermore, the evolution and chronostratigraphic significance of the basal surfaces underlying MTCs in areas of recurrent mass-wasting has not been studied previously.

This study is based on detailed mapping of the near-seabed, likely Pleistocene stratigraphy (Ortiz-Karpp et al., 2015), imaged in a 3D seismic reflection survey from the southern Magdalena Fan, offshore Colombia (Fig. 1). The seismic survey is located at the northern tip of the Southern Sinú Fold Belt, imaging the transition between imbricate thrust-cored anticlines to the south and a relatively undeformed area to the north (Fig. 1B). Here, several MTCs were deposited at a time when the Magdalena Fan was prograding under the influence of high sediment supply and the Southern Sinú Fold Belt was propagating outboard to the NW (e.g. Romero-Otero et al., 2009; Martinez et al., 2015). Due to the location of the study area within the fold-and-thrust belt and to the relatively recent tectonic deformation of the near-seabed sediments, the degree of deformation is less advanced than in other areas along the fold-and-thrust belt (Vinnels et al., 2010; Romero-Otero et al., 2010; Alfaro & Holz, 2014); the primary tectono-stratigraphic relationships and internal characteristics of the deposits are therefore well-preserved. The high-resolution of the data and its tectono-stratigraphic setting therefore enable: i) the examination of variations in the distribution, source and size of the MTCs in response to growth of the deep-water fold-and-thrust belt, and ii) the investigation of the evolution and chronostratigraphic significance of MTC basal erosion surfaces.

2. Regional Setting

The Magdalena Fan is located in the Caribbean Sea, on the northern coast of Colombia, northern South America (Fig. 1). The margin is tectonically active due to Cretaceous-to-Recent oblique subduction of the Caribbean Plate beneath the South American Plate (Duque-Caro, 1979; Pindell, 1994; Meschede & Frisch, 1998; Cediél et al., 2003; Pindell & Kennan, 2009). Plate convergence has resulted in the formation of imbricate thrust belts, which have been active onshore since the Late Paleocene (Flinch, 2003) and offshore since the Middle-Late Miocene (Cediél et al., 2003; Martinez et al., 2015). The offshore Sinú Fold Belt is dominated by a series of thrust-cored anticlines that young to the north (Bernal-Olaya, 2015; Martinez et al., 2015) and have experienced episodic growth during the Plio-Pleistocene (Kolla & Buffler, 1984; Duque-Caro, 1979; 1984; Cediél et al., 2003; Flinch, 2003). The Sinú Fold Belt is divided into two regions of active deformation (Southern & Northern Sinú fold belts; Fig. 1B). The Magdalena Fan, which is believed to have been active

since the Late Miocene (Duque-Caro, 1979; 1984; Kolla & Buffler, 1984; Breen, 1989; Romero-Otero, 2009), is located in a relatively undeformed area between the fold belts, extending offshore into the Colombia Basin (Fig. 1B). Submarine fan sedimentation was coeval with subduction-induced structural uplift and tectonic activity (Kolla & Buffler, 1984; Vinnels et al., 2010; Romero-Otero 2009; Romero-Otero et al., 2010; Alfaro & Holz, 2014; Ortiz-Karpf et al., 2015).

3. Data and Methods

This study uses a three-dimensional seismic reflection survey covering the northern tip of the Southern Sinú Fold Belt and the southern part of the undeformed area that is mantled by the Magdalena Fan (Fig. 1B). The seismic survey was acquired in 2008 and covers an area of 1900 km². It is Post-Stack Depth-Migrated (PSDM) and has a bin spacing of 12.5 x 12.5 m. This study focuses on the shallow stratigraphy (up to c. 1,000 m below seabed) where the maximum frequency is 45 Hz and the dominant frequency is 30 Hz. By assuming a sediment velocity of 1900 m/s, which seems reasonable given the relatively shallow depth of burial, these frequency and velocity values yield a vertical resolution of c. 10-15 m and a horizontal resolution of c. 15 m. The water bottom is defined by a positive reflection event, which is represented by a black reflection in the presented seismic images. Although a few wells have been drilled to the NE of the study area, they were not available for this study.

Ortiz-Karpf et al. (2015) studied the stratigraphic interval of interest, defining seven seismic facies that were used to infer a number of sedimentary sub-environments (i.e. channel-fill, levees, lobes and MTCs). These sub-environments were then grouped into seven seismic units. Ortiz-Karpf et al. (2015) interpret that seismic Unit D, which is located 300-500 m below the seabed, is dominated by MTCs. In the study described here, Unit D and older, underlying MTCs and their bounding surfaces were characterised and mapped in greater detail, and the chronology of MTC emplacement was assessed with respect to the development of the deep-water fold-and-thrust belt. Based on the amplitude, continuity and configuration of the reflections, and their external geometry, three MTC seismic facies are defined (Table 1). Attribute extractions, including amplitude, dip, variance and chaos were performed and integrated with variance and amplitude depth slices to define lateral facies changes and create seismic facies maps. Kinematic indicators such as the orientation of the lateral scarps, onlap patterns, fold and fault vergence, grooves and megaclasts alignment (*sensu* Bull et al., 2009) were interpreted from maps and cross-sectional views. These kinematic indicators were used to infer MTC flow directions and to link individual MTCs back to their source areas, thus enabling the investigation of the relationship between fold-and-thrust belt growth, seabed deformation and MTC emplacement.

4. Structural elements

In order to relate the characteristics of the MTCs to the structural evolution, it is necessary to establish the structural framework of the study area. This section describes the structures whose growth led to or controlled emplacement of the MTCs.

Towards the northern tip of the southern Sinú Fold Belt, NE-SW-striking thrusts bend towards the east, resulting in an overall rotation of the deformation front towards the continent (Figs. 1B & 2). Within the study area, two thrust sheets are imaged (Fig. 2). Basinwards three more thrust sheets are present to the SW of the seismic volume (Fig. 2). In the study area, the western and eastern thrust sheets are each associated with large anticlines, herein referred to as the *downdip anticline (DA)* and *updip anticline (UA)* respectively (Fig. 2). These anticlines are separated by a narrow syncline, herein referred to as the *syncline* (Fig. 3).

The DA is divided into a northern and southern domain, which are separated by a saddle (Fig. 3A). The southern downdip anticline (SDA), is asymmetric, with its steepest flank dipping to the NW. The anticline is cored by the *southern fault zone (SFZ)*, which comprises three sub-parallel thrust faults that strike SW-NE and dip to the SE (Fig. 3A & C). The relief of the anticline increases to the SW, and the displacement, strike and lateral separation of the underlying faults vary. Towards the NE, the faults curve towards the east (Fig. 3A), become steeper, and lose displacement before ultimately tipping out.

Towards the northern tip of the SFZ, the DA becomes progressively more symmetric, and its axis rotates towards the east (Fig. 3A). Here the anticline plunges slightly to the NE to form the saddle (Fig. 3D) separating it from the northern downdip anticline (NDA). Towards the NE the axis of the anticline rotates towards the east (Fig. 3A) and the anticline becomes broad and symmetric (Fig. 3A & B). The NDA is unfaulted and it does not have a seabed expression because it has been greatly eroded (Fig. 3B).

The UA is a narrow, thrust-cored, asymmetric anticline that verges to the NW with a sub-vertical to overturned frontal limb (Fig. 3C). The UA is expressed at the seabed, although its geometry has been modified by erosion (Fig. 3C). The thrust coring the UA also curves to the east and continues to the NE, bending towards the shelf (Fig. 2 & 3A).

According to Martinez et al. (2015), the structures in the study area have experienced episodic growth since the Late Miocene. This protracted growth history is evidenced by thinning of the stratigraphic packages against the DA and UA, and increased sediment thickness into the syncline (Fig. 3B & C), which together indicate the presence of growth

strata. Because these folds have deformed the seabed, and their underlying thrusts displace shallow stratigraphy (Fig. 3C), the last period of uplift of these structures is interpreted to have occurred relatively recently and potentially coincides with the latest stage of offshore uplift, associated with the Late Pleistocene avulsion of the Magdalena River (Romero-Otero, 2009). However, the youngest MTCs and the overlying channel-levee complex sets are not faulted and onlap the downdip anticline (Fig. 3C). This reflects a period of tectonic quiescence and active fan sedimentation post-dating the latest episode of fold and thrust activity.

5. Seismic Stratigraphy

The base and top surfaces of Unit D (*sensu* Ortiz-Karpf et al., 2015) are continuous negative-amplitude reflections that can be mapped throughout the study area and bound several MTCs (Fig. 4). Here, the stratigraphy within Unit D is subdivided based on mappable surfaces. To facilitate the description of the MTCs, the area was divided into three regions based on the morphology of the erosion surface that defines the base of Unit D (Fig. 4): i) the *southern region*, which is located basinward of the SDA, and to the NE of two thrust sheets that terminate to the south of the dataset (Fig. 4A & B); ii) the *central region*, which trends SW along the axis of the syncline, NW across the downdip anticline at the saddle between the SDA and NDA, and covers the basin-low outboard of the downdip anticline (Fig. 4B); and (iii) the *northern region*, which traverses the NDA (Fig. 4B). The nomenclature adopted for the individual MTCs described below is based on the region where they occur and on their relative age with respect to other MTCs in the same region. Thus, the MTCs in the southern region are named S1-S6, the MTC in the central region is referred to as C1, and those in the northern region are called N1 and N2. With the exception of S1-S4 and the MTC remnants underlying C1, the MTCs described below form part of Unit D of Ortiz-Karpf et al. (2015) (Fig. 4C). Table 2 summarises the dimensions, seismic facies, megaclast dimensions and kinematic indicators associated with each of the MTCs.

5.1 Southern Region:

The southern region contains six stacked MTCs that are mainly composed of debrites and megaclasts (Fig. 5, Table 2); these are elongate in a NE-SW direction and are the oldest MTCs in the study interval (S1-S6; Fig. 4 & 5). S1-S5 continue beyond the southwestern limit of the dataset where the southern fault zone curves to the west and where two additional thrust sheets, located west of the downdip anticline, plunge to the north (Fig. 4A).

MTC S1 is located towards the southern limit of the dataset and is only locally preserved due to erosion, folding and faulting (Fig. 5A). Towards the north it onlaps and erodes an

underlying external levee. It is truncated by S2 (Fig. 6A). Structural deformation hinders the identification of its eastern depositional limit, seismic facies, or the transport direction.

MTC S2 overlies an erosion surface that incises S1 and is erosionally overlain by S3 (Fig. 6A). S2 onlaps and erodes the external levee of an underlying channel complex set (Fig. 6A) extending farther north than S1 (Fig. 5B). S2 thins towards the north and west (Fig. 6C) and is folded and faulted to the SE, thinning against the frontal flank of the SDA (Fig. 7A & B). In the thicker central area, S2 is characterised by variable amplitudes, and towards the margins it displays lower amplitudes and is more homogenous (Fig. 5B & 6C). Megaclasts in S2 are concentrated in the central part of the deposit and are aligned SW-NE, broadly sub-parallel to the margins (Fig. 5B & 6C). The megaclasts are folded but the sense of fold vergence is unclear.

MTC S3 overlies an erosion surface that incises S2 although, locally, they are separated by erosional remnants of a package of low-amplitude reflections (Fig. 6A). S3 is top-truncated by S5 (Fig. 6A) and, in the north, by S4 (Fig. 5D). S3 onlaps and erodes the underlying external levee towards the north, and is folded and faulted to the SE where it thins against the western flank of the SDA (Figs. 6A & D, 7A & B). Amplitudes are variable towards the central area; more homogenous, lower amplitudes characterise the northern margin (Fig. 5C & 6D). Most of the megaclasts in S3 are aligned NE-SW, parallel to the northwestern margin (Fig. 5C & 6D) and are internally folded. The vergence of the folds within the megaclasts is not clear.

MTC S4 is located to the NW of S1-S3 (Fig. 5D & 6D). It overlies and incises into the axes and levee crests of two SW-trending channel-levee complex sets (Fig. 6A & D(i)). The southeastern external levee of one of these channel-levee complex sets separates S4 from S3 (Fig. 5D & 6D). To the NW, S4 overlies the remnant external levee that constitutes the limit between the southern and central regions (Fig. 5D). S4 is truncated by S5 to the SW, by S6 to the NE and truncates S3 (Fig. 5D-E, 6A & 8A-B). S4 can be traced updip onto the SDA, where it is folded, faulted (Fig. 8A) and truncated by C1 (Fig. 5D). S4 is composed of two packages separated by a laterally continuous, high-amplitude erosion surface that suggests the presence of two stacked MTCs (Fig. 8A); both are composed of debrites with few megaclasts (Fig. 5D & 6D). The megaclasts are concentrated in the SW (Fig. 5D). The orientation of the lateral boundaries of S4, which follow the trend of underlying channel-levee complex sets, suggest deposition from a NE- or SW-directed flow (Fig. 6D); however there are no additional kinematic indicators to support either interpretation.

MTC S5 overlies an erosion surface that incises S3 and S4 (Fig. 6A). To the NW, as in S4, it is limited by the external levee deposits that define the boundary between the southern and

central regions (Fig. 5E). To the NE, S5 thins and pinches-out against the underlying channel levee complex set and is erosionally truncated by S6 (Fig. 6A & 8A). To the east it thins against the SDA where it is folded and faulted (Fig. 7A-B). S5 has an irregular top that is overlain and locally eroded by channel-levee complex sets to the south (Fig. 7 A-B). S5 is composed of debrites towards the margins and, in its centre, by continuous reflections that form asymmetric to recumbent, NE-verging folds contained within deformed megaclasts (Figs. 5E & 7A & D). To the NE, the transition from folded facies to debrite coincides with the shallowing of the basal surface and thinning of the deposit (Fig. 7C-E). Based on the orientation of the axes of the folds within the megaclasts (WNW-ESE; Fig. 7D), their NNE fold vergence (Fig. 8B), and the presence of erosional scours and grooves at the base of S5 (Fig. 7C), the emplacement direction of the flow depositing S5 is interpreted to be towards the NNE.

MTC S6 overlies an erosion surface that incises S5 and S4 (Fig. 8A-B), and is overlain by channel-levee complex sets (Fig. 8). As in S4 and S5, to the NW, it thins against the external levee that defines the boundary between the southern and central regions (Figs. 5F & 8D); although an erosion surface can locally be observed between MTC S6 and MTC C1 (Fig. 5), it is not consistently traceable, meaning it is possible that S6 is part of C1 (Fig. 6A). To the SW, S6 thins and pinches-out against relief developed along the upper surface of S5 (Fig. 5G & 8). To the NE, the basal erosion surface can be traced to the tip of the southern fault zone where it overlies S4 and amalgamates with the erosion surface bounding the base of C1 (Fig. 5F & 8A). Unlike S1-S5, S6 is not offset by the faults in the southern fault zone and the channel-levee complexes that overlie it are undeformed (Fig. 8A-B). S6 mainly comprises debrites and folded megaclasts (Fig. 5F & 8C), being c. 100 m thick towards its centre and thinning away from this point in all directions (Fig. 8D). The overall widening of the deposit to the SW and its southwestern termination against S5 suggest deposition from a SW-directed flow.

5.2 Central Region.

Only one laterally extensive MTC (C1) is developed in the central region. C1 overlies a major erosion surface that trends along the syncline, cross-cuts the downdip anticline in the saddle area and extends into the basin-low to the west (Fig. 9A-B). In the syncline, the lateral walls to C1 are steep and formed by the back limb of the NDA and the frontal limb of the UA (Fig. 9D). Basinward of the downdip anticline, C1 is bounded to the SE by the external levee remnant that separates the southern and the central regions, and to the NW by the southern external levee of an underlying SW-trending channel-levee complex set (Fig. 9E). C1 covers an area of c. 300 km² and its basal surface covers c. 400 km² with the height of its lateral

margins decreasing in the downdip direction from c. 500 m to c. 120 m (Fig. 9D & E). C1 is not incorporated into or deformed by the fold-and-thrust belt, and is overlain by channel-levee complex sets that onlap the MTC and the flanking anticlines (Fig. 9C).

C1 is mainly composed of debrites and it is also internally deformed by imbricate thrusts and folds, which are concentrated towards the centre of the deposit where it is thickest (up to 200 m) (Fig. 9A-C). Towards its margins, the deposit is thinner (up to 50 m) and consists of lower-amplitude debrites (Fig. 9A-B). The deposit thins to ≤ 50 m across the downdip anticline, where it contains abundant megaclasts in a thin matrix formed by debrites (Fig. 9). Megaclasts are identified throughout C1 and are internally folded (Fig. 9B & E).

In the syncline, thrusts within C1 dip to the NE (Fig. 9C), suggesting emplacement by a SW-directed flow, an interpretation supported by the SW orientation of the lateral scarps (Fig. 9A-B). Further downdip, in the basin-low, thrusts dip to the SE (Fig. 9C), indicating emplacement by a broadly NW-directed flow. This inferred emplacement direction is supported by the NW-SE strike orientation of the lateral scarps, which is interpreted to be broadly parallel to the overall flow direction (*cf.* Bull et al., 2009). Further downdip, towards the western edge of the dataset, the orientation of the lateral scarps changes to WSW, suggesting C1 was emplaced by a WSW-directed flow (Fig. 9A). Therefore, although the overall trend of MTC C1 is roughly WNW, there were local variations in the direction of the flow.

The stratigraphy underlying C1 is folded and comprises channel-levee complex sets and MTCs (Fig. 9C). Towards the toe of the frontal limb of the DA, at the tip of the southern fault zone, a SW-trending erosional surface overlain by thin MTC remnants is locally preserved beneath C1 (Fig. 9C). Due to subsequent erosion its updip limit cannot be established. In the syncline, the strata underlying C1, thin against the flanks (Fig. 10B). Updip of the NDA, folded MTC remnants underlying C1 are elongate NE-SW, and overlie and erode the axial portion of a SW-trending channel-levee complex set that is also folded (Fig. 10A & B). Given that the MTCs are only locally preserved their emplacement direction is uncertain. However, because the MTCs and the underlying channel-levee complex are folded and follow a similar trend, it is more likely that the MTCs were emplaced by a SW-directed flow. The southern part of the syncline contains stacked MTCs that thin against the fold flanks and are interpreted to be younger than those in the northern part of the syncline (Fig. 10D). The older MTCs in the southern part of the syncline are displaced by the thrusts that core the UA and are folded into the back limb of the SDA, with the degree of stratal rotation decreasing upward (Fig. 10C). There are also younger, undeformed MTCs that overly C1 (Fig. 10D). Irrespective of their relative age, all the MTCs in the southern part of the syncline are

elongate SW-NE and can be mapped to the steep frontal limb of the UA, which is thus interpreted to be their source (Fig. 10A & D).

5.3 Northern Region

The northern region traverses the NDA (Fig. 4) and contains two MTCs that overlie erosion surfaces (N1 and N2) (Fig. 4). N1 is truncated by N2, and thins updip where the two bounding erosion surfaces merge; no MTCs are documented above the clearly erosional basal surface, suggesting a zone of sediment bypass (e.g. Stevenson et al., 2015; Fig. 11B). The composite erosion surface incised c. 300 m into the northern part of the NDA and truncates several folded stratigraphic packages (Fig. 11B). Updip of the NDA, the composite surface directly overlies and erodes a channel-levee complex set, and across the western limb of the anticline it is bounded on either side by channel-levee complex sets (Fig. 11B-C). Further downdip, N1 underlies C1 and is capped by N2 (Fig. 11B); the downdip extent of N2 is controlled by irregular relief formed by megaclasts in C1 (Fig. 11B).

N1 and N2 are up to c. 90 m thick and are composed of debrites (Fig. 11A- Table 2). They contain several laterally discontinuous erosion surfaces, suggesting these deposits are the result of multiple periods of erosion and deposition. Along the northern lateral wall, arcuate scarps visible on variance extractions (Fig. 11A) coincide with a terrace-like geometry to the basal surface (Fig. 11C). These discontinuous erosion surfaces are overlain by debrites and are therefore interpreted to have been formed by gravitational collapse of the northern lateral wall, a process that probably contributed to the southward shift and progressive widening of the basal erosion surface (Fig. 11C).

Based on the orientation of the lateral scarps, N1 and N2 are interpreted to have been deposited by WSW-directed flows. N1 and N2 truncate underlying folded stratigraphy; they are not folded and are overlain by onlapping, undeformed channel-levee complex sets (Fig. 11B). The stratigraphic packages underlying N1 and N2, which include thin (50-90 m thick) stacked MTCs, thin against the western flank of the DA (Fig. 11D).

6. Interpretation.

6.1. MTC provenance and timing of emplacement

Figure 12A summarises the chronostratigraphic relationship between the different MTCs and the growth history of individual structures in the fold-and-thrust belt. In the southern region, S1-S5 are folded and displaced across the thrusts coring the SDA (Fig. 7A-B), indicating

they were deposited before the most recent phase of faulting and folding. Furthermore, eastward thinning of S1-S5 against the western flank of the SDA suggests that some structural relief existed prior to the emplacement of MTCs S1-S5 and that they are likely syn-tectonic (Fig. 12A). In contrast, S6 is not faulted or folded, and is overlain by largely undeformed channel-levee complex sets that passively onlap the flanking anticlines (Fig. 8B); S6 is therefore interpreted as post-tectonic. In the central region, the MTCs pre-dating C1 in the syncline are folded and thin against the flanks (Fig. 10), and they are therefore interpreted as syn-tectonic. C1 is post-tectonic because it is undeformed and is overlapped by undeformed channel-levee complex sets (Fig. 9C); it therefore defines the transition from syn- to post-tectonic sediments. In the southern part of the syncline, the transition from folded and faulted MTCs, to undeformed MTCs occurs at a similar stratigraphic level to C1 (Fig. 10C-D), indicating that the UA and DA were active at broadly the same time. Similarly, in the northern region, N1 and N2 are underlain by MTCs that thin against the NDA suggesting that they are syn-tectonic (Fig. 11D). Conversely, N1 and N2 are themselves undeformed and overlain by undeformed, onlapping channel-levee complex sets and are therefore post-tectonic (Fig. 11B). The age relationship between syn-tectonic MTCs in the southern, central and northern regions cannot be established with confidence.

The emplacement direction of the southern MTCs is challenging to constrain with confidence because the MTCs extend to the SW of the study area (Fig. 5). S5 contains the most convincing kinematic indicators, which together support an emplacement direction towards the NNE (Fig. 12B): NNE orientated grooves and scours at the base (Fig. 7C), and NE-verging folds within megaclasts (Fig. 8B) with WNW-ESE orientated fold axes (Fig. 7D). The elongate morphology of S1-S3 (Fig. 5), their northward onlap against the underlying levee (Fig. 6A) and the NE-SW alignment of the megaclasts in S2-S3 (Fig. 5 & 6B-D) also suggest this emplacement direction. Therefore, MTCs S1-S3 and S5 could have been sourced from local collapse of the southern part of the SDA or other anticlines to the SW of the dataset (Fig. 12B). MTCs S1-S3 and S5 are thus classified as detached MTCs (*sensu* Moscardelli and Wood, 2008). Estimated runout distances for MTCs S1-S3 could be c. 10, 15 and 20 km, respectively. The abrupt increase in quantity and size of megaclasts in S5 (Table 2) could reflect a shorter runout distance and it is more likely that S5 was sourced from the southern part of the SDA (Fig. 12B). Similar mass-wasting of deep-water fold-and-thrust belts has been documented south of the study area (Vinnels et al., 2010; Romero-Otero et al., 2010; Alfaro & Holz, 2014). The provenance of S4 is uncertain because there are no flow direction indicators, its northeastern portion is folded and eroded by S6 and C1 (Figs. 8A), and it is only partially imaged by the seismic survey. S4 may have been also sourced from the SW. Alternatively, given that it follows the trend of underlying channel-levee complex

sets, it could also have been sourced from the northern part of the SDA or even further updip, depending on the structural relief of the SDA at the time of emplacement. S6 was emplaced from the NE. It can be traced to the tip of the southern fault zone but, because it is eroded by C1, the updip limit of its headwall is not preserved (Fig. 8C), and it is unclear whether it was sourced from the frontal flank of the SDA or if it traversed the anticline and was sourced from further updip (Fig. 12B).

Based on the orientation of the lateral scarps and the vergence of the faults in the imbricate fold and thrust systems (Fig. 9), C1 is interpreted to have been emplaced by a broadly WNW-trending flow. C1 extends beyond the eastern limit of the dataset, where the present-day bathymetry shows arcuate scarps on the shelf break, analogous to the 'cookie-bite' features described by Moscardelli & Wood (2008; Fig. 12B). The shelf break thus represents the potential source area for C1, suggesting this deposit is best classified as a shelf-attached MTC (*sensu* Moscardelli & Wood, 2008). There are multiple possible sources for the syn-tectonic MTCs that underlie C1 in the syncline. Towards the southern part of the syncline, MTCs were sourced from the frontal flank of the UA and were directed to the NE (Figs. 10 & 12B). There are also some MTCs that post-date C1, indicating several stages of mass-wasting of the UA. In the northern part of the syncline, the syn-tectonic MTC remnants are interpreted to have been sourced from the NE because they are elongated parallel to the syncline and the underlying SW-trending channel-levee complex sets (Fig. 10A). However, it is not possible to establish whether they were sourced from the shelf or from other collapses along the frontal limb of the UA. It is also unclear whether the MTCs in the syncline traversed the DA into the basin-low. However, given that these MTCs are relatively small and that there is scarce evidence of older MTCs underlying C1 in the basin-low outboard of the DA (Figs. 10A & 13A-C), it is inferred that they were confined to the small basin defined by the syncline.

Based on the orientation of the lateral scarps, N1 and N2 are interpreted to have been deposited by WSW-directed flows and to have been sourced from the NE. Like C1, N1 and N2 are located directly downdip of the arcuate scarps on the shelf break (Fig. 12B); these MTCs are accordingly interpreted to have been sourced from the shelf and are classified as shelf-attached MTCs (*sensu* Moscardelli and Wood, 2008). The syn-tectonic MTCs underlying N1 and N2 (Fig. 11D) were likely sourced from the frontal flank of the NDA (Fig. 12B) and are therefore classified as detached MTCs (*sensu* Moscardelli & Wood, 2008).

6.2. Tectono-stratigraphic Evolution

Figure 13 summarises the interpreted link between growth of the deep-water fold-and-thrust belt and the emplacement of genetically-related MTCs. Before the latest phase of activity on

the thrusts that core the UA and the DA, MTCs in the southern region were mostly sourced from the SW, where the flanks of the anticlines were steeper (Fig. 13A). As the SDA grew, S1 became folded and S2 was emplaced occupying a greater area and extending further to the NE (Table 2). The MTCs deposited in the syncline were mainly sourced from the UA and are interpreted to have been confined to the mini-basin bounded by the DA and UA (Fig. 13A). This interpretation is supported by the presence of growth strata, which indicates that the DA and UA had been uplifted and degraded to some extent, by the scarce and thin MTC remnants found at the toe of the DA (Fig. 9C), and by the small size of the detached MTCs that occupy the syncline (Fig. 10). Nonetheless, it remains possible that some flows, possibly including S6, traversed the structure prior to the emplacement of C1, potentially across the lower relief saddle between the SDA and NDA, and that the deposits associated with these flows were subsequently eroded by C1.

As the anticlines grew, the syncline and areas basinward of the DA were filled by MTCs derived from the degradation of the growing structures (Fig. 13B): S3 occupied a greater area and extended further N than S2 (Table 2, Fig. 12B), S4 was emplaced to the NW of S1-S3, and syn-tectonic MTCs were sourced from the frontal limb of the DA (Fig. 13B).

S5 was the last and largest MTC sourced from the SW and it was likely derived from the southern part of the SDA (Fig. 13C). It eroded S3 and S4 and extended further to the NE. After S5 was emplaced, thin-skinned shortening and folding culminated with faulting of both fold cores (Fig. 13C). Faulting would have generated further instability due to steepening of the anticline frontal limbs. S6 was then deposited; it could have been sourced from the frontal limb of the DA or derived further updip (Fig. 13C). N1 was also emplaced after tectonic activity had stopped in that area, being deposited along the trend of a long-lived sediment flow-pathway defined by stacked channel-levee complex sets (Fig. 13C). The DA was degraded progressively by erosion of the back limb of the SDA and possibly by retrogradational collapse of the frontal limb (Fig. 13C).

The cessation of tectonic activity would have led to decreased accommodation as the syncline filled. Decreased accommodation and degradation of the folds at the saddle between the SDA and NDA would have allowed larger, shelf-attached MTCs to traverse the anticline, establishing a conduit between the syncline and the deep basin (Fig. 13D). In the northern region N2 followed the trend of N1, leading to widening of the erosion surface.

Progressive degradation of the DA by several erosional flows that were initially confined in the syncline eventually connected the shelf break with the basin-low downdip of the structures. Previous studies document similar breaching of the folds bounding mini-basins by MTCs (e.g. Vinnels et al., 2010; Geersen et al., 2011). Based on data from offshore Chile,

Geersen et al. (2011) propose a model for the breaching of a thrust-cored high formed between the shelf and an offshore anticline. They propose that structural uplift led to oversteepening of the frontal flank of the anticline until a critical angle was reached, at which time mass-wasting, possibly triggered by an earthquake, smoothed the slope profile and reconnected the shelf with the slope. Vinnels et al. (2010), recognise comparable processes to the SW of the current study area associated with repeated back-stepping slope failures that connected otherwise isolated piggyback basins developed in the evolving Sinú Fold Belt.

7. Discussion

7.1. Changes in MTC distribution, source and size in response to structural uplift

Deposition of syn-tectonic MTCs (S1-S5) shifted progressively to the NE, likely reflecting changes in source area. After the last episode of uplift, which culminated in propagation of the faults that core the DA and the UA, MTC source areas shifted towards the NE closer to the shelf-break, and shelf-attached MTCs were emplaced (MTCs C1, N1 and N2). These change could have been controlled by the evolution of the structures, or could be attributed to externally-driven, more regional controls, such as increased sediment supply, eustatic sea-level change, gas hydrate dissolution and/or seismicity (e.g. Manley and Flood, 1988; Beaubouef and Friedmann, 2000; Maslin et al., 2004; Frey Martinez et al., 2005; Grozic, 2010; Masson et al., 2010; Alfaro and Holz, 2014). Along the northern coast of Colombia, during the Pleistocene, uplift of the Sinú Fold Belt was accompanied by uplift of the northern Andes, which coincided with changes in eustatic sea-level and regional climate (Van der Hammen, 1958; 1974; Duque-Caro, 1979; Hooghiemstra & Ran, 1994; Ortiz-Karpf et al., 2015). Also, in the Plio-Pleistocene, there were nine avulsions of the Magdalena River (Romero-Otero, 2009), which would have caused abrupt changes in sediment input and dispersal patterns. Therefore, several external forcing mechanisms can be invoked for the emplacement of the shelf-attached MTCs (Ortiz-Karpf et al., 2015). However, the UA bends to the east towards the area of the shelf where the arcuate scarps, interpreted as a possible source for the shelf-attached MTCs, are located (Fig. 12B). It is therefore likely that uplift associated with the propagation of the thrust that cores the UA induced the development of steep, unstable areas close to the shelf.

The results of this study suggest a northward shift in the source area of the MTCs through time, coinciding with the propagation direction of the structures (e.g. Martinez et al., 2015; Bernal-Olaya, 2015). This local finding suggests that systematic shifts in MTC source areas through time could be investigated in other areas along the margin to help constrain the evolution of the entire Sinú Fold Belt. Previous studies in other basin margins also report

systematic variations in the morphology and distribution of syn-tectonic sedimentary packages with continued structural uplift. In the Apennines, Festa et al. (2015) also observed systematic shifts in the occurrence of MTCs in the direction of propagation of the fold-and-thrust-belt, and an increase in the volume of the MTCs through time. In the Niger Delta, variations in the architecture, morphology and distribution of MTCs and channel-levee complex sets were also documented in a syn-tectonic stratigraphic package in the vicinity of a fold (Clark and Cartwright, 2010; 2012); these variations were used to constrain the evolution of the fold (Clark and Cartwright, 2012). These observations suggest that systematic, fold-belt-driven shifts in MTC source areas are reflected in the morphology, distribution and characteristics of the deposit, and that this link is common to both active and passive margins. The results presented here are thus potentially applicable to other fold-and-thrust belts around the world.

Changes in source are reflected in the size of the MTCs: the syn-tectonic MTCs are detached and cover areas of c. 9-100 km² within the study area (Table 2); the post-tectonic MTCs are shelf-attached and have areal extents of at least 200-300 km² (Table 2). These findings are in accordance with those of Moscardelli & Wood (2008; 2015), who found that detached MTCs have areas of tens of km² whereas attached MTCs can be hundreds to thousands of km² in area. The difference between the volumes of detached and shelf-attached MTCs can be readily explained by considering the volumes of material available at the source; these volumes are likely to be smaller along local flank collapses than on the delta-fed shelf break. However, the evolution of the seascape during degradation and sedimentation can also play an important role in the areal extent, runout distance and therefore the distribution of MTCs. For example, in the southern region, there is a progressive increase in the area and down-flow extent of the syn-tectonic, detached MTCs (S1-S5-Table 2). This could be explained by the sequential steepening of the frontal limbs of the growing anticlines, which could have resulted in progressively larger failures. Also, the emplacement of earlier MTCs immediately down-dip of the forelimb would have smoothed the break-in-slope contributing to the progressively longer runout distances and larger areal extents. The greater areal extents and runout distances of the shelf attached MTCs (C1, N1 and N2, Table 2) are also the result of the smoothed the slope profile through progressive degradation of the folds. The distribution, morphology and scale of the resulting MTCs therefore reflect changes in source areas induced by the combined effects of structural growth and syn-tectonic and post-tectonic degradation of the thrust-and-fold belt. Such changes in external MTC characteristics should also be reflected in their internal composition, impacting their ability to act as hydrocarbon reservoirs or seals (e.g. Gamboa et al., 2010; Omosanya & Alves, 2013; Alves et al., 2014).

7.2. Evolution and chronostratigraphic significance of MTC basal surfaces.

The recent tectono-stratigraphic evolution of the fold-and-thrust belt resulted in the formation of an erosion surface that is overlain by at least 9 distinct MTCs (Fig. 13). This composite, surface was widened and deepened by multiple erosional flows and is therefore time-transgressive. The basal surface developed during a period dominated by thin-skinned contraction, folding and thrusting, and syn- and post-tectonic fold degradation, presumably over a protracted period of time. In addition to the specific MTCs identified and described, local collapse of the lateral walls, evidenced by the arcuate scarps at the margins of the basal surfaces of N1 and N2 (Fig. 411C), also contributed to widening the composite basal erosion surface.

Previous studies suggest that time-transgressive MTC basal surfaces are common. Using 3D seismic from offshore Israel, Frey-Martinez et al. (2005) document at least three large-scale slumps related to, and emplaced on a continuous basal shear surface. On the Exmouth Plateau, Scarselli et al. (2013) report a series of MTCs in the Late Pliocene-Recent stratigraphy, interpreting that the different orientations of grooves in the basal surface to reflect different transport directions resulting from the multi-stage evolution of the complex. The models for syn-tectonic fold degradation presented by Heniö & Davies (2006) and Geersen et al. (2011) also imply repeated episodes of mass-wasting and sedimentation. Therefore, despite the quasi-instantaneous emplacement of individual MTCs, their deposits may coalesce above composite basal surfaces that are time-transgressive. In other words, these composite basal surfaces are transferred into the rock record, but probably never were a geomorphic surface (cf. Strong and Paola, 2008).

The identification of discrete MTCs is likely limited by dataset resolution. For instance, the basal surface of Unit D (Ortiz-Karpf et al., 2015), which is overlain by MTCs of various ages, is a continuous reflection that can be mapped across the study area (Fig. 4). At deeper burial depths the composite nature of similar erosion surfaces at the base of multiple stacked MTCs might not be resolvable, and thus be interpreted as a geomorphic surface overlain by a single MTC, obscuring the complex tectono-stratigraphic history that led to its formation. Distinguishing between single and composite MTC basal surfaces can impact the interpretation of sedimentary basin burial histories, which are commonly used to evaluate the timing of hydrocarbon generation and expulsion. It can also influence the prediction of the characteristics and distribution of the sedimentary packages downdip of the MTCs. Furthermore, the presence of coalescing MTCs can introduce lateral facies variability and affect the prediction of sealing capacity (e.g. Gamboa et al., 2010; Omosanya & Alves, 2013; Alves et al., 2014). Hence, this study illustrates the potential complexity of deeper

subsurface examples where the development of the MTC basal surfaces and the tectono-stratigraphic history may not be resolvable.

8. Conclusions

Detached and shelf-attached MTCs are recognised in the northern tip of the southern Sinú deep-water fold-and-thrust belt. Detached MTCs are mainly syn-tectonic, are mostly sourced from the SW, and in the southern region have minimum areal extents of c. 9 to 100 km². The post-tectonic MTCs are shelf-attached and cover areas in excess of 300 km².

The characteristics of the MTCs reflect changes in source area through time and help constrain the complex tectono-stratigraphic history of the study area. The direction in which the MTC source areas shifted through time coincides with the direction of propagation of the anticlines, suggesting that structural evolution was an important control on the distribution and characteristics of the MTCs. Similar observations in other active and passive basin margins suggest that systematic shifts in MTC source areas as fold-and-thrust-belts evolve are possibly generic and that a similar approach could be applied to help constrain the evolution of fold-and-thrust belts elsewhere.

The unconformity represented by the erosion surface at the base of the MTC package is composite and time-transgressive, forming over a protracted period of slope instability associated with the punctuated growth of the deep-water fold-and-thrust belt. Therefore, despite the quasi-instantaneous emplacement of individual MTCs, MTC basal surfaces may have longer and more complex histories in locations subject to repeated mass-flows, with implications for interpretations of burial history, the heterogeneity of the MTCs themselves and inferences regarding downdip sedimentation. The studied system may be a valuable analogue for deeper subsurface examples where the development of MTC basal surfaces and the tectono-stratigraphic evolution may not be resolvable.

Acknowledgements

The authors wish to thank Shell, Ecopetrol S.A. and Petrobras for supplying the dataset used in this study and Colciencias for providing the funding for the first author. We would also like to thank Davide Gamboa and Jose-Frey Martinez whose comments and suggestions helped to greatly improve this paper.

Conflict of Interest

No conflict of interest declared

References

- ALFARO, E. & HOLZ, M. (2014) Seismic geomorphological analysis of deepwater gravity-driven deposits on a slope system of the southern Colombian Caribbean margin. *Mar. Pet. Geol.* 57, 294-311.
- ALVES, T. M., KURTEV, K., MOORE, G. F. & STRASSER, M. (2014) Assessing the internal character, reservoir potential, and seal competence of mass-transport deposits using seismic texture: A geophysical and petrophysical approach. *AAPG Bull.*, 98 (4), 793-824.
- ALVES, T. (2015) Submarine slide blocks and associated soft-sediment deformation in deep-water basins: A review. *Mar. Pet. Geol.*, 67, 262-285.
- BEAUBOUEF, R.T. & FRIEDMANN, S.J. (2000). High resolution seismic/sequence stratigraphic framework for the evolution of Pleistocene intra slope basins, western Gulf of Mexico: depositional models and reservoir analogs. In: *Deep-water Reservoirs of the World*, (Ed. by P. Weimer, R.M. Slatt, J. Coleman, N.C. Rosen, H. Nelson, A.H Bouma, M.J. Styzen, and D.T. Lawrence), Gulf Coast Section SEPM 20th Annual Research Conference, 40-60.
- BERNAL-OLAYA, R., SANCHEZ, J., MANN, P. & MURPHY, M. (2015) Along-strike crustal thickness variations of the subducting Caribbean Plate produces two distinctive styles of thrusting in the offshore South Caribbean Deformed Belt, Colombia. In: *Petroleum geology and potential of the Colombian Caribbean margin*, (Ed. by C. Bartolini and P., Mann), *AAPG Mem.*, 108, 295-322.
- BULL, S. & CARTWRIGHT, J. (2010) Small-Scale Insights into Seismic-Scale Slumps: A Comparison of Slump Features from the Waitemata Basin, New Zealand, and the Møre Basin, Off-Shore Norway. In: *Submarine Mass Movements and Their Consequences*, 2010 (Ed. by D.C. Mosher, R.C. Shipp, , L. Moscardelli, , J.D. Chaytor, C.D.P. Baxter, H.J. Lee, and R. Urgeles), Springer, Netherlands, 257–266.

- BULL, S., CARTWRIGHT, J. & HUUSE, M. (2009) A review of kinematic indicators from mass-transport complexes using 3D seismic data. *Mar. Pet. Geol.*, 26 (7), 1132-1151.
- BREEN, N. A. (1989) Structural effect of Magdalena fan deposition on the northern Colombia convergent margin. *Geology*, 17 (1), 34–37.
- CATTANEO, A., BABONNEAU, N., DAN, G., DÉVERCHÈRE, J., DOMZIG, A., GAULLIER, V., LEPILLIER, B., DE LÉPINARY, B.M., NOUGUÈS, A., STRZERZYNSKI, P., SULTAN, N. & YELLES, K. (2010) Submarine landslides along the Algerian margin: A review of their occurrence and potential link with tectonic structures. In: *Submarine Mass Movements and Their Consequences*, 2010 (Ed. by D.C. Mosher, R.C. Shipp, , L. Moscardelli, , J.D. Chaytor, , C.D.P., Baxter, H.J. Lee, and R. Urgeles), Springer, Netherlands, 515–525.
- CEDIÉL, F., SHAW, R. P. & CÁCERES, C. (2003) Tectonic assembly of the Northern Andean Block. In: *The Circum-Gulf of Mexico and the Caribbean: Hydrocarbon habitats, basin formation, and plate tectonics* (Ed. by C. Bartolini, R. T. Buffler, and J. Blickwede). *AAPG Mem.*, 79, 815– 848.
- CLARK, I.R. & CARTRIGHT, J.A. (2009) Interactions between submarine channel systems and deformation in deepwater fold belts: Examples from the Levant Basin, Eastern Mediterranean sea. *Mar. Pet. Geol.*, 26, 1465–1482.
- CLARK, I.R. & CARTRIGHT, J.A. (2012) Interactions between coeval sedimentation and deformation from the Niger delta deepwater fold belt. In: *Application of the Principles Seismic Geomorphology to Continental Slope and Base-of-slope Systems: Case Studies from Seafloor and Near-Seafloor Analogues*, (Ed. by B. E. Prather, M. E. Deptuck, D. Mohrig, B. van Hoorn and R. B. Wynn), *SEPM Spec.Publ.*, 99, 243-267.
- DAN, G., SULTAN, N., CATTANEO, A., DÉVERCHÈRE, J. & YELLES, K. (2010) Mass-transport deposits on the Algerian margin (Algiers area): Morphology, lithology and sedimentary processes. In: *Submarine Mass Movements and Their Consequences*, 2010, (Ed. by D.C. Mosher, R.C. Shipp, , L. Moscardelli, , J.D. Chaytor, , C.D.P., Baxter, H.J. Lee, and R. Urgeles), Springer, Netherlands, 527–539.
- DOTT., R.H Jr. (1963) Dynamics of Subaqueous Gravity Depositional Processes. *AAPG Bull.* 47 (1), 104-128.

- DUQUE-CARO, H. (1979) Major structural elements and evolution of northwestern Colombia. In: *Geological and Geophysical Investigations of Continental Margins*, (Ed. by J.S. Watkins, L. Montadert, and P.W. Dickerson), *AAPG Mem.*, 29, 329-351.
- DUQUE-CARO, H. (1984) Structural style, diapirism, and accretionary episodes of the Sinú-San Jacinto terrane, southwestern Caribbean borderland: *Geol. Soc. Am. Mem.*, 162, 303–316.
- FESTA, A., OGATA, KEI., PINI, G.A., DILEK, Y & CODEGONE, G (2015) Late Oligocene-early Miocene olistostromes (sedimentary mélanges) as tectonostratigraphic constraints to the geodynamic evolution of the exhumed Ligurian accretionary complex (Northern Apennines, NW Italy), *Int. Geol. Rev.*, 57 (5-8), 540-562.
- FLINCH, J. F. (2003) Structural evolution of the Sinú-Lower Magdalena area (northern Colombia). In: *The Circum-Gulf of Mexico and the Caribbean: Hydrocarbon habitats, basin formation, and plate tectonics* (Ed. by C. Bartolini, R. T. Buffler, and J. Blickwede), *AAPG Mem.*, 79, 776–796.
- FREY-MARTINEZ, J. (2010) 3D Seismic interpretation of mass transport deposits: Implications for basin analysis and geohazard evaluation. In: *Submarine Mass Movements and Their Consequences* (Ed. by D.C. Mosher, R.C. Shipp, , L. Moscardelli, , J.D. Chaytor, , C.D.P., Baxter, H.J. Lee, and R. Urgeles), Springer, Netherlands, 553–568.
- FREY-MARTINEZ, J., CARTWRIGHT, J., & HALL, B. (2005) 3D seismic interpretation of slump complexes: Examples from the continental margin of Israel. *Basin Res.*, 17 (1), 83–108.
- FREY-MARTINEZ, J., CARTWRIGHT, J., & JAMES, D. (2006) Frontally confined versus frontally emergent submarine landslides: A 3D seismic characterisation. *Mar. Pet. Geol.*, 23, 585–604.
- GAMBOA, D., ALVES, T., CARTWRIGHT, J. & TERRINHA, P. (2010) MTD distribution on a 'passive' continental margin: the Espírito Santo Basin (SE Brazil) during the Palaeogene. *Mar. Pet. Geol.*, 27 (7), 1311-1324.
- GEERSEN, J., VÖLKER, D., BEHRMANN, J.H., REICHERT, C., & KRASTEL, S. (2011) Pleistocene giant slope failures offshore Arauco Peninsula, Southern Chile. *J. Geol. Soc.*, 168, 1237–1248.

- GOLDFINGER, C., KULM, L.V.D., MCNEILL, L.C., & WATTS, P. (2000) Super-scale failure of the southern Oregon Cascadia margin. *Pure and Applied Geophysics*, 157, 1189–1226.
- GROZIC, J.L.H. (2010) Interplay between gas hydrates and submarine slope failure. In: *Submarine Mass Movements and Their Consequences*, (Ed. by D.C. Mosher, R.C. Shipp, L. Moscardelli, J.D. Chaytor, C.D.P., Baxter, H.J. Lee, and R. Urgeles), Springer, Netherlands, 11-30.
- HEINIÖ, P. & DAVIES, R.J. (2006). Degradation of compressional fold belts: deep-water Niger Delta. *AAPG Bull.*, 90, 753–770.
- HOOGHIEMSTRA, H. & RAN, E.T. (1994) Late and middle Pleistocene climatic change and forest development in Colombia: pollen record Funza II (2-158 m core interval). *Palaeogeogr. Palaeocl.* 109 (2), 211-246.
- IDÁRRAGA-GARCÍA, J. & VARGAS, C.A. (2014) Morphological Expression of Submarine Landslides in the Accretionary Prism of the Caribbean Continental Margin of Colombia. In: *Submarine Mass Movements and Their Consequences*, 2014, (Ed. by S. Krastel, J.H. Behrmann, M. Stripp, C. Berndt, R. Urgeles, J. Chaytor, K. Huhn, M. Strasser and C. Bonnevie Harbitz), Springer International Publishing, Switzerland.
- JACKSON, C.A.-L. (2011) Three-dimensional seismic analysis of megaclast deformation within a mass transport deposit; implications for debris flow kinematics. *Geology* 39, 203-206.
- JONES, O.T. (1939) The geology of the Colwyn Bay district: study of submarine slumping during the Salopian Period. *Q. J. Geol. Soc.*, 95, 335-382.
- KOLLA, V., & BUFFLER, R.T. (1984) Morphologic, acoustic, and sedimentologic characteristics of the Magdalena Fan. *Geo-Mar. Lett.*, 3, 85-91.
- LAMARCHE, G., JOANNE, C., & COLLOT, J. Y. (2008) Successive, large mass-transport deposits in the south Kermadec fore-arc basin, New Zealand: The Matakaoa Submarine Instability Complex. *Geochem. Geophys. Geosyst.*, 9, Q04001.
- MANICA, R. (2012) Sediment Gravity Flows: Study Based on Experimental Simulations. In: *Hydrodynamics -Natural Water Bodies* (Ed. by H. Schulz, H., Simões, A., and Lobosco, R.), 263-286.

- MANLEY, P.L. & FLOOD, R.D. (1988). Cyclic deposition within Amazon deep-sea fan. *AAPG Bull.*, 72, 912-925.
- MARTINEZ., J., CASTILLO., J., ORTIZ-KARPF, A., RENDON, L., MOSQUERA, J.C. & VEGA, V. (2015) Deep Water Untested Oil-Play in the Magdalena Fan, Caribbean, Colombian Basin. In: *Petroleum geology and potential of the Colombian Caribbean margin*, (Ed. by C. Bartolini and P., Mann), *AAPG Mem.*, 108, 251-260.
- MASLIN, M., OWEN, M., DAY, S., & LONG, D. (2004). Linking continental-slope failures and climate change: testing the clathrate gun hypothesis. *Geology*, 32 (1), 53-56.
- MASSON, D.G., WYNN, R.B., TALLING, P.J., 2010. Large landslides on passive continental margins: processes, hypotheses and outstanding questions. In: *Submarine Mass Movements and Their Consequences*, (Ed. by D.C. Mosher, R.C. Shipp, , L. Moscardelli, , J.D. Chaytor, , C.D.P., Baxter, H.J. Lee, and R. Urgeles), Springer, Netherlands, 153-166.
- MCGILVERY, T. A., HADDAD, G., & COOK, D. L. (2004). Seafloor and shallow subsurface examples of mass transport complexes, offshore Brunei. In: *Offshore Technology Conference*. Offshore Technology Conference.
- MESCHEDE, M. & FRISCH, W. (1998) A plate-tectonic model for the Mesozoic and early Cenozoic history of the Caribbean plate. *Tectonophysics*, 296 (3), 269–291.
- MINISINI, D., TRINCARDI, F., ASIOLI, A., CANU, M., & FOGLINI, F. (2007) Morphologic variability of exposed mass-transport deposits on the eastern slope of Gela Basin (Sicily channel). *Basin Res.*, 19, 217–240.
- MOORE, D.G., CURRAY, J.R., & EMMEL, F.J. (1976) Large submarine slide (olistostrome) associated with Sunda Arc subduction zone, northeast Indian Ocean. *Mar. Geol.*, 21, 211–226.
- MOSCARDELLI, L., WOOD, L. & MANN, P. (2006) Mass-transport complexes and associated processes in the offshore area of Trinidad and Venezuela. *AAPG Bull.* 90 (7), 1059-1088.
- MOSCARDELLI, L. & WOOD, L. (2008) New classification system for mass transport complexes in offshore Trinidad. *Basin Res.*, 20 (1), 73-98.
- MOSCARDELLI, L. & WOOD, L. (2015) Morphometry of mass-transport deposits as a predictive tool. *Geol. Soc. Am. Bul.*, B31221-1.

- NEMEC, W. (1990) Aspects of sediment movement on steep delta slopes. In: *Coarse-Grained Deltas* (Ed. by A. Colella and D.B. Prior), *Spec. Publs. Int. Ass. Sediment.*, 10, 29-73.
- OLAFIRANYE, K., JACKSON, C.A.-L. & HODGSON, D.M. (2013) The role of tectonics and mass-transport complex emplacement on upper slope stratigraphic evolution: a 3D seismic case study from offshore Angola. *Mar. Pet. Geol.* 44, 196-216.
- OMOSANYA, K. O. & ALVES, T. M (2013) A 3-dimensional seismic method to assess the provenance of mass-transport deposits (MTDs) on salt-rich continental slopes (Espírito Santo Basin, SE Brazil). *Mar. Pet. Geol.*, 44, 223-239.
- ORTIZ-KARPF, A., HODGSON, D. M., & MCCAFFREY, W. D. (2015) The role of mass-transport complexes in controlling channel avulsion and the subsequent sediment dispersal patterns on an active margin: The Magdalena Fan, offshore Colombia. *Mar. Pet. Geol.* 64, 58-75.
- PÉREZ, L. F., BOHOYO, F., HERNÁNDEZ-MOLINA, F.J., CASAS, D., GALINDO-ZALDÍVAR, J., RUANO, P., & MALDONADO, A (2016), Tectonic activity evolution of the Scotia-Antarctic Plate boundary from mass transport deposit analysis. *J. Geophys. Res. Solid Earth*, 121, 2216–2234.
- PINDELL, J. L. (1994) Evolution of the Gulf of Mexico and the Caribbean: In: *Caribbean geology. An introduction*, (Ed. by S.K., Donovan and T.A. Jackson), University of the West Indies Publisher's association, 13–39.
- PINDELL, J. L. & KENNAN, L. (2009) Tectonic evolution of the Gulf of Mexico, Caribbean and northern South America in the mantle reference frame: An update. *Spec. Publ. Geol. Soc. London*, 328 (1), 1–55.
- POSAMENTIER, H.W. & KOLLA, V. (2003) Seismic geomorphology and stratigraphy of depositional elements in deep-water settings. *J. Sediment. Res.* 73 (3), 367-388.
- POSAMENTIER, H.W. & MARTINSEN, O.J. (2011) The character and genesis of submarine mass-transport deposits: insights from outcrop and 3D seismic data. In: *Mass-transport Deposits in Deepwater Settings* (Ed. by R.G. Shipp, P. Weimer, H.W. Posamentier), *Spec. Publ. SEPM*, 96, 7-38.
- ROGERS, K.G. & GOODBRED, S.L. (2010) Mass failures associated with the passage of a large tropical cyclone over the Swatch of No Ground submarine canyon (Bay of Bengal). *Geology*, 38, 1051–1054.

- ROMERO-OTERO, G.A. (2009) Deepwater Sedimentary Processes in an Active Margin, Magdalena Submarine Fan, Offshore Colombia (PhD thesis). University of Oklahoma, 298 p.
- ROMERO-OTERO, G.A., SLATT, R.M. & PIRMEZ, C. (2010) Detached and shelf-attached mass transport complexes on the Magdalena deepwater fan. In: *Submarine Mass Movements and Their Consequences*, (Ed. by D.C. Mosher, R.C. Shipp, L. Moscardelli, J.D. Chaytor, C.D.P., Baxter, H.J. Lee, and R. Urgeles), Springer, Netherlands, 593-606.
- SCARSELLI, N., MCCLAY, K. & ELDERS, C. (2013) Submarine Slide and Slump Complexes, Exmouth Plateau, NW Shelf of Australia, In: *Western Australian Basins Symposium 2013*, Aug 18-21 2013 Perth, (Ed. by Keep, M. & Moss, S.J), Petroleum Exploration Society of Australia.
- SHANMUGAM, G., LEHTONEN, L.R., STRAUME, T., SYVERTSEN, S.E., HODGKINSON, R. J. & SKIBELI, M. (1994) Slump and Debris-Flow Dominated Upper Slope Facies in the Cretaceous of the Norwegian and Northern North Seas (61–67°N): Implications for Sand Distribution. *AAPG Bull.* 78 (6), 910-937.
- STEVENSON, C., JACKSON, C.L., HODGSON, D.M., HUBBARD, S. M & EGGENHUISEN, J. (2015) Deep-water sediment bypass. *J. Sediment. Res.*, 85, 1058-1081.
- STRONG, N. & PAOLA, C. (2008) Valleys that never were: time surfaces versus stratigraphic surfaces: *J. Sediment. Res.*, 78, 579-593.
- TORELLI, L., SARTORI, R., & ZITELLINI, N., (1997) The giant chaotic body in the Atlantic Ocean off Gibraltar: New results from a deep seismic reflection survey. *Mar. Pet. Geol.*, 14, 125–138.
- TRINCARDI, F., & ARGNANI, A. (1990) Gela submarine slide: A major basin-wide event in the Plio-Quaternary foredeep of Sicily. *Geo-Mar. Lett.*, 10, 13–21.
- VARGAS, C.A. & IDÁRRAGA-GARCÍA, J. (2014) Age Estimation of Submarine Landslides in the La Aguja Submarine Canyon, Northwestern Colombia. In: *Submarine Mass Movements and Their Consequences, 2014*, (Ed. by S. Krastel, J.H. Behrmann, M. Stripp, C. Berndt, R. Urgeles, J. Chaytor, K. Huhn, M. Strasser and C. Bonnevie Harbitz), Springer International Publishing, Switzerland.

- VAN DER HAMMEN, T. (1958) Estratigrafía del Terciario y Maestrichtiano continentales y tectogénesis de los Andes Colombianos. *Boletín Geológico Ingeominas* 6 (1-3), 67-128.
- VAN DER HAMMEN, T. (1974) The Pleistocene changes of vegetation and climate in tropical South America. *J. Biogeogr.*, 3-26.
- VINNELS, J.S., BUTLER, R.W.H., MCCAFFREY, W.D., & PATON, D.A. (2010) Depositional processes across the Sinú accretionary prism, offshore Colombia. *Mar. Pet. Geol.* 27 (4), 794-809.
- WEIMER, P. (1990) Sequence stratigraphy, seismic geometries, and depositional history of the Mississippi Fan, deep Gulf of Mexico. *AAPG Bull.*, 74, 425-453.
- WOODCOCK, N.H. (1976) Structural style in slump sheets: Ludlow Series, Powys, Wales. *J. Geol. Soc.*, 132, 399-415.
- YARBUH, I. & CONTRERAS, J. (2015) The interplay between deformation, erosion and sedimentation in the deep-water Mexican Ridges foldbelt, western Gulf of Mexico basin. *Basin Res.* doi:10.1111/bre.12157.

Figure Captions

Figure 1. Location and tectonic setting. **A.** The Magdalena Fan is located in the Caribbean Sea, off the northern coast of Colombia, South America where the Caribbean Plate obliquely subducts beneath the South American Plate. The yellow polygon outlines the Magdalena Fan (*cf.* Kolla & Buffler, 1984), map from NOAA. **B.** The Magdalena Fan is in the Sinú Fold Belt, which is divided into the Southern Sinú Fold Belt (SSFB) and the Northern Sinú Fold Belt (NSFB), separated by an area of subduced deformation. Adapted from Romero-Otero (2009).

Table 1. MTC seismic facies. **A.** Description and interpretation of the seismic facies. **B.** Variance extraction of the upper part of an MTC (see A for intersection) showing the appearance of facies 1 and 2. **C.** Seismic line across B showing examples of facies 1 and 2. **D.** Depth-slice showing the map-view appearance of a large folded megaclast. Note the semi continuous folded reflections and the fold axis. **E.** Seismic line across D. Note the asymmetry of the folds. **F.** Seismic line across facies 1 and 3. Note the imbricate fold-and-thrust systems in facies 3. **G.** Seismic line showing facies 2.

Figure 2. Subregional structural setting. Seabed dip map coloured by subsurface elevation within the seismic volume. The main thrusts and anticlinal axis in and around the study area

are from Romero-Otero (2009). The study area is in the northern tip of the Southern Sinú Fold Belt and images two thrust sheets, the downdip anticline (DA) and updip anticline (UA).

Figure 3. Structural elements. **A.** Three dimensional perspective view of the seismic cube (see B-D for depth intersection). The southern downdip anticline (SDA) is thrust-cored, the northern downdip anticline (NDA) is not faulted. A saddle separates the SDA and the NDA. To the E, there is a syncline (S) that separates the DA and the updip anticline (UA). **B.** Dip seismic line across the northern part of the dataset: The NDA becomes symmetric and is not faulted. There is increased sediment thickness in the syncline (S). **C.** Dip seismic line across the southern part of the dataset: The SDA is thrust-cored and asymmetric, to the E is the UA. **D.** Seismic line along the axis of the downdip anticline. There is a saddle between the SDA and NDA. Note thinning of the sedimentary packages against the SDA.

Figure 4. MTC Regions. **A.** Location of the MTC regions with respect to the main thrusts and folds around the area; axes of anticlines expressed on the seabed taken from Romero-Otero (2009). The black polygon indicates the location of the study area; the polygons defining the limits of the MTC regions are projected vertically onto the seabed. The southern region is to the west of the southern downdip anticline (SDA), the central region traverses the saddle between the SDA and the northern downdip anticline (NDA), and the northern region traverses the NDA. Towards the E of the dataset is the updip anticline (UA). **B.** Combined display of variance and elevation on the base surface of Unit D, the orange horizon in C (cf. Ortiz-Karpf et al., 2015). **C.** Oblique seismic line across the MTC regions; the orange horizon corresponds to the erosional surface mapped in B and the yellow horizon is the top of the MTC package. Unit D of Ortiz- Karpf et al. (2015) corresponds to the interval between the red and yellow horizons.

Table 2. Summary table showing the main characteristics of the MTCs and their classification according to the interpreted source and timing with respect to the evolution of the anticlines.

Figure 5. Maps showing the areal distribution, morphology and seismic facies distribution of MTCs S1-S6. Projected vertically onto a depth slice, refer to Fig. 6A for intersection.

Figure 6. **A.** Strike line along the southern region, see Fig. 5 & 6B-D for location. MTCs S1-S3 overlap an underlying external levee. S4 overlies a channel-levee complex set. S5 pinches out to the north and S6 pinches out to the south against megaclasts protruding at the top of S5. **B-D.** i) Variance depth slices across MTCs S1, S2 and S3 respectively showing the distribution of the seismic facies; see A for intersection), ii) Vertical thickness maps for S1, S2 and S3. **E.** Vertical thickness map for MTC S4.

Figure 7. **A.** Uninterpreted cross-section across S1-S5 showing examples of the seismic facies. For location refer to B-E and Fig. 5. **B.** Geo-seismic cross-section showing the deformation of S1-S5 by the southern fault zone (SFZ) and the western limb of the southern downdip anticline (SDA). **C.** Variance extraction at the base of S5 showing lineaments interpreted as erosional scours and grooves. **D.** Amplitude depth slice across S5 showing the distribution of the seismic facies; see A for intersection **E.** Vertical thickness map for S5.

Figure 8. MTCs S4 & S6. **A.** Seismic line along S4 showing examples of the seismic facies. For location refer to C and 5D. Note the deformation of S4 across the southern fault zone (SFZ) and the western limb of the southern downdip anticline (SDA). **B.** Seismic line along

S6. For location refer to C and Fig. 5F. S6 pinches to the south against protrusions on the top of S5; to the E it is undeformed. Note the geometry of the folded megaclasts in S5, which is used to interpret a NNE-directed flow. S6 is interpreted to have been emplaced by a SW-directed flow. CLCs are channel-levee complex sets. **C.** Variance depth slice (see B for intersection) showing the geometry and seismic facies within S6. **D.** Vertical thickness map for S6.

Figure 9. MTC C1. **A.** Thickness map of C1. Note that C1 thins towards its margins and across the downdip anticline (DA). **B.** Facies map of C1. **C.** Seismic line along C1 showing the variation of the seismic facies along strike. Note the MTC remnant underlying C1 at the toe of the SDA and the thinning across the anticline. C1 is not structurally deformed. CLCs denote channel-levee complex sets. **D.** Seismic line across the constriction of C1 showing examples of the seismic facies. The underfilled basal surface of C1 was filled by onlapping, undeformed CLCs. **E.** Oblique seismic line towards the western limit of the dataset showing examples of folded megaclasts, note the decrease in the relief of the erosion surface with respect to D.

Figure 10. MTCs underlying C1. **A.** Map showing the distribution of the MTCs that underlie C1 (grey polygons). **B.** Seismic cross-section across the northern part of the syncline where several stacked MTCs underlie C1. They overlie a channel-levee complex set and are folded and faulted into the northern downdip anticline (NDA) and the updip anticline (UA). **C.** Seismic cross-section across the southern part of the syncline, which is filled by several MTCs. The older MTCs are faulted and folded into the SDA and the UA. The younger MTCs are undeformed. **D.** Seismic line along the syncline. The MTCs that underlie C1 in the northern part overlie a CLC and are older than those in the southern part of the syncline. The MTCs in the southern part of the syncline can be traced to the western flank of the UA. To the N, they are truncated by C1. There is also evidence of MTCs sourced from the UA in the stratigraphy overlying C1.

Figure 11. MTCs N1 and N2. **A.** Variance extraction at the base of N1 overlain by seismic facies maps for N1 and N2, which are mainly composed of facies 1. Note the arcuate scarps (AS) visible on the variance extraction. **B.** Seismic line along the northern region. N1 and N2 traverse the northern downdip anticline (NDA); the stratigraphy underlying the erosion surfaces of N1 and N2 is folded while the stratigraphy overlying them is undeformed. Note that N1 is eroded by N2 and that N1 underlies C1 while N2 overlies it. The downdip extent of N2 is controlled by protrusions at the top of C1. Updip, there is an area of bypass. **C.** Seismic line across the arcuate scarps shown in A. They coincide with a “terraced” geometry, which is interpreted to reflect slumping from the northern lateral wall. N1 and N2 overlie channel-levee complex sets (CLCs). **D.** Close up of B on the NDA showing thinning against the flanks of the anticline and MTCs that can be traced to the western limb of the NDA.

Figure 12. Summary of interpreted chronostratigraphy and provenance. **A.** Chronostratigraphic chart of the MTCs and their relative timing with respect to the tectonic events. In the southern region, MTCs S1-S5 were deposited before faulting and during folding and are classified as syn-tectonic. S6-N2 were deposited after folding and faulting had ceased and are post-tectonic. The relative timing between S6 and N1 cannot be established. In the central region, the MTCs underlying C1 were deposited during folding and possibly during faulting; they are syn-tectonic. **B.** Map showing the interpreted source

areas for the syn-tectonic MTCs (i.e. S1-S5 and the MTCs underlying C1 and N1/N2), and the post-tectonic MTCs (i.e. C1, N1 and N2). Most of the syn-tectonic MTCs were sourced from the flanks of the growing anticlines and are classified as detached (*sensu* Moscardelli and Wood, 2008), while the post-tectonic MTCs (C1, N1-N2) are shelf-attached (*sensu* Moscardelli and Wood, 2008).

Figure 13. Schematic representation of the tectono-stratigraphic evolution. **A.** MTCs were potentially ponded in the syncline sourced mainly from the frontal limb of the updip anticline (UA). MTCs in the northern part of the syncline may have been sourced from the UA or the shelf. S1 and S2 were sourced from the SW of the dataset. The northern region contained a channel-levee complex set (CLC). **B.** As uplift continued S3 and S4, and more MTCs in the syncline were deposited. Stacking of the MTCs created composite basal erosion surfaces. **C.** Emplacement of S5 was followed by faulting. As structural uplift ceased, the syncline was filled by MTCs that eroded the back limb of the downdip anticline and further enlarged the composite basal surface. Back-stepping erosion of MTCs from the frontal flank may have contributed to the degradation of the DA. It is not clear if S6 was connected to the syncline or sourced from the frontal limb of the SDA. N1 exploited and widened the CLC in the northern region. **D.** C1 traversed the DA creating a through-going composite surface that connected the basin-low and the syncline. This surface amalgamated with the basal surface in the southern region creating an even larger composite surface. N2 was also sourced from the shelf.

Figure 1.

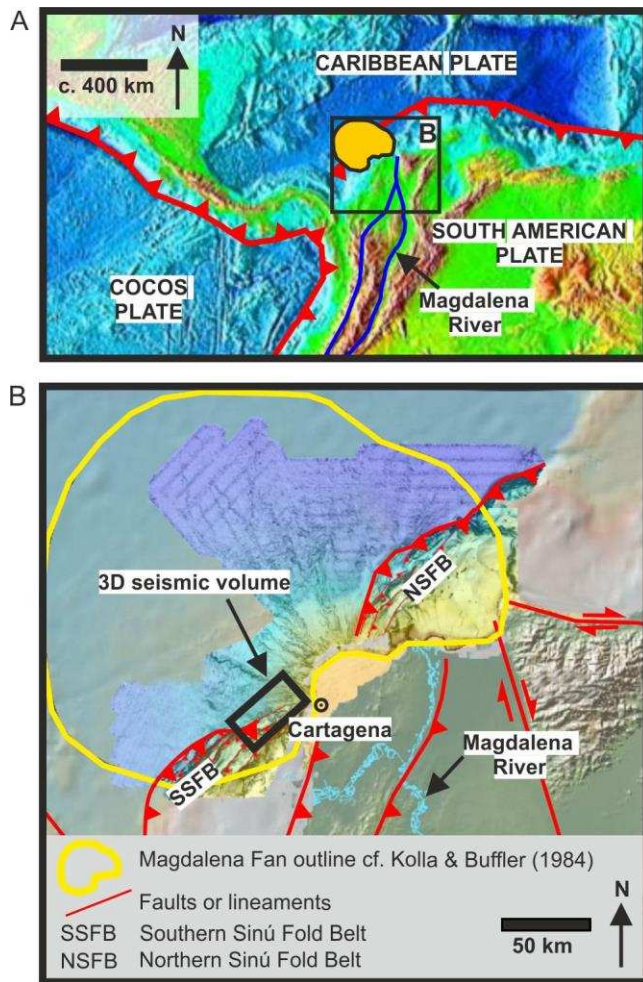


Table 1.

A		
Seismic Facies	Description	Interpretation
①	Variable amplitude, semi-continuous to chaotic reflections in packages that have an erosional base and irregular top (B-C). Packages are 50-100 m thick and are sometimes locally deformed by thrusts and 200-300 m wide folds.	The chaotic character of facies 1 suggests that the contained material is at least partially disaggregated (cf. Alves et al., 2014) and, based on these characteristics, facies 1 is interpreted to represent debrites (cf. Posamentier & Kolla, 2003; Olafiranye et al., 2013).
②	Discrete packages of coherent, parallel reflections set within a matrix dominated by facies 1 (B-C). These coherent reflections occur in packages that are predominantly up to 200 m thick and cover areas of up to 1.6 km ² . In some cases these packages are folded or faulted. Some of these packages are considerably larger, with areas of 5-7 km ² and thicknesses in excess of 300 m. They are composed of parallel reflections that are folded into symmetric, asymmetric, recumbent and isoclinal folds and are associated with facies 1 (D-E).	Megaclasts transported within the MTC parent flow (e.g. Olafiranye et al., 2013; Jackson, 2011; Ortiz-Karpf et al., 2015). Due to the lateral continuity of the reflections and the scale of the folds, the larger packages could be alternatively interpreted as slump folds (cf. Bull & Cartwright, 2010; Posamentier & Martinsen, 2011). However, differentiating between these two hypotheses is not critical to the overall objective of this study and they are also interpreted as megaclasts (cf. McGilvery et al., 2004; Bull et al., 2009; Frey-Martinez, 2010; Jackson, 2011; Posamentier & Martinsen, 2011; Olafiranye et al., 2013; Alves, 2015). The geometry of the folds can be used to infer the MTC flow direction, with the fold axes interpreted to be orientated broadly perpendicular to flow direction and the folds verging in the down-flow direction (cf. Jones, 1939; Woodcock, 1976; Bull et al., 2009). When the folds are symmetric, only the azimuth of the flow can be determined.
③	Variable amplitude, semi-continuous reflections that are folded and disrupted by reverse faults (F). Thrust imbricates which commonly bound asymmetric anticlines are well developed in facies 3. The folds are 400-500 m wide and c. 200 m high.	Imbricate thrust and fold systems (<i>sensu</i> Bull et al., 2009) in contractionally deformed MTCs (e.g. McGilvery et al., 2004; Frey-Martinez et al., 2005; 2006; Alfaro & Holz, 2014). Flow direction is generally perpendicular to the strike of the faults and folds verge in the down-flow direction (Bull et al., 2009).

Figure B: Seismic reflection image showing facies 1 (chaotic reflections) and facies 2 (coherent reflections). A 2 km scale bar is present. Axes X-X' and X-X' are indicated.

Figure C: Seismic reflection image showing facies 1 and 2. A 500 m scale bar is present. Axes X-X' and B-C are indicated.

Figure D: Seismic reflection image showing facies 2. A 2 km scale bar is present. Axes Z-Z' and Flow direction are indicated.

Figure E: Seismic reflection image showing facies 2. A 1 km scale bar is present. Axes Z-Z' and Flow direction are indicated.

Figure F: Seismic reflection image showing facies 1 and 3. A 1 km scale bar is present. Axes Z-Z' and Flow direction are indicated.

Figure G: Seismic reflection image showing facies 2. A 500 m scale bar is present. Axes Z-Z' and Flow direction are indicated.

Figure 2.

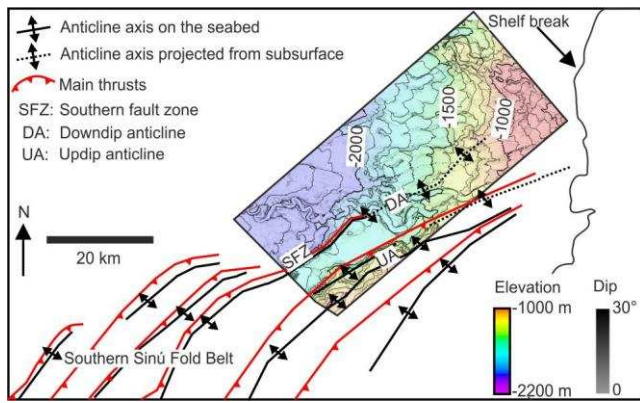


Figure 3.

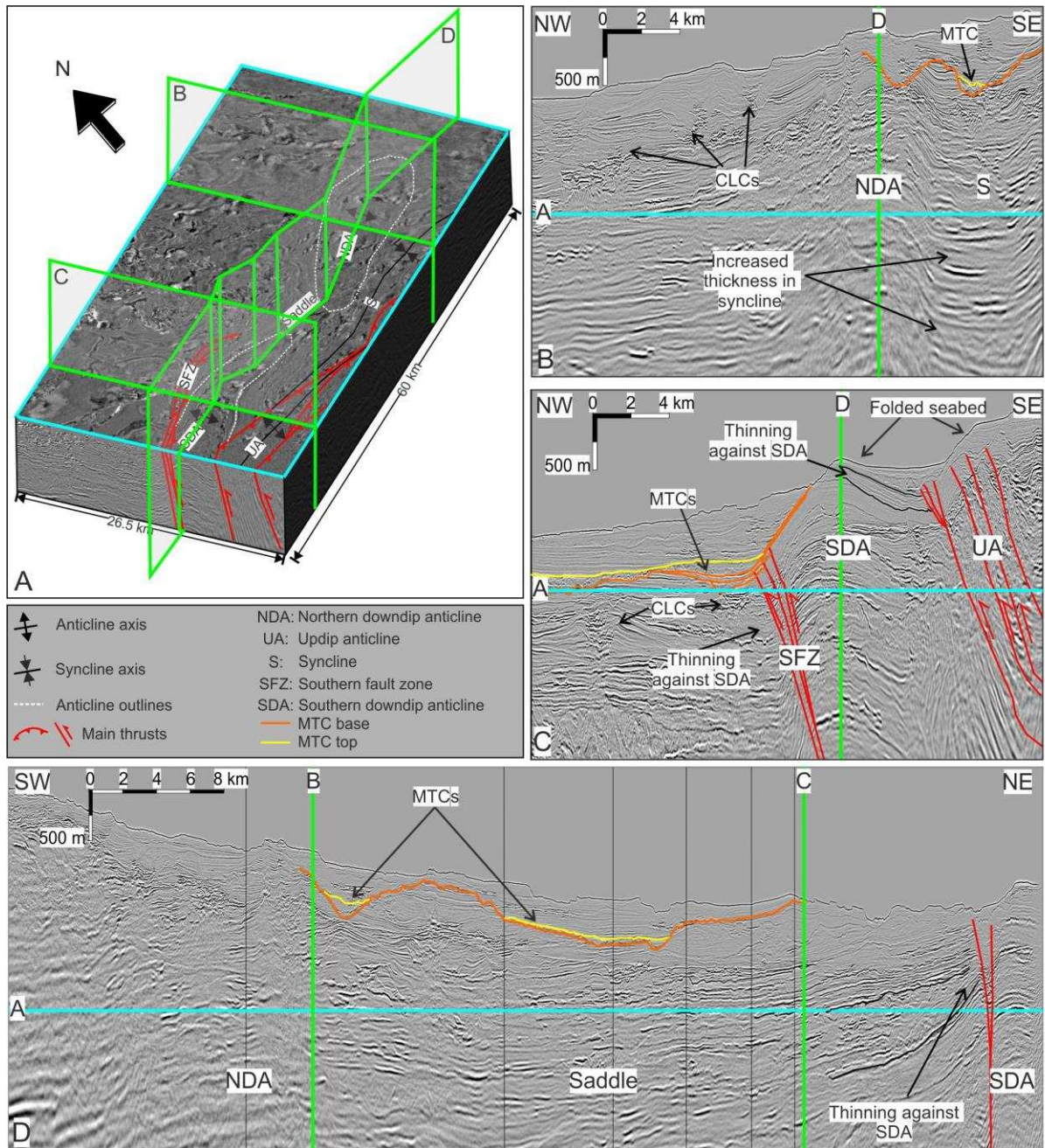


Figure 4.

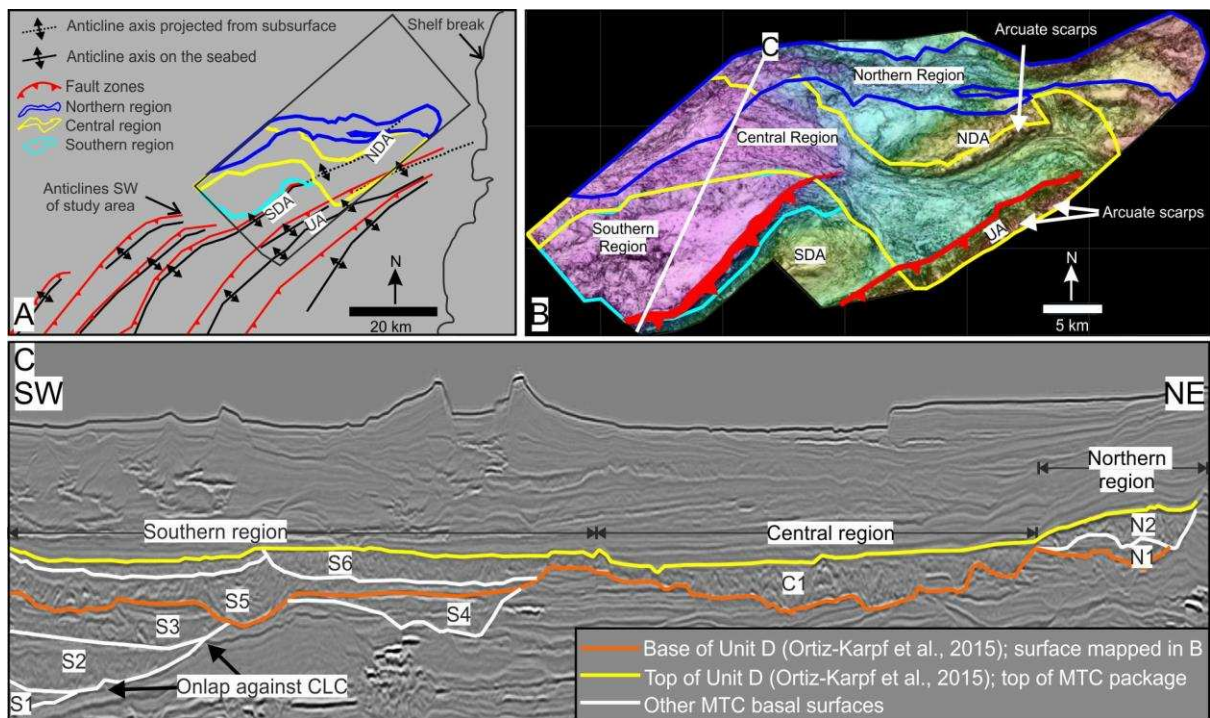


Table 2.

	MTC	Thickness (m)	Minimum Dimensions (within study area)	Seismic facies	Size of megaclasts	Kinematic Indicators
Syn-tectonic Detached	S1	25-150	Length: 5 km Width: 2 km Area: 9 km ²	Obscured by tectonic deformation	None identified	NE-SW elongation; progressive onlap against channel levee to the N
	S2	20-150	Length: 8 km Width: 5 km Area: 30 km ²	Facies 1 (debrites) and facies 2 (megaclasts)	Thickness: 80-130 m Area: 0.3 km ²	NE-SW elongation; progressive onlap against channel levee to the N, alignment of megaclasts
	S3	30-100	Length: 9 km Width: 5 km Area: 42 km ²	Facies 1 (debrites) and facies 2 (megaclasts)	Thickness: 50-90 m Area: 0.06-0.35 km ²	NE-SW elongation; progressive onlap against channel levee to the N, alignment of megaclasts
	S4	30-130	Length: 19 km Width: 6 km Area: 75 km ²	Facies 1 (debrites) and facies 2 (megaclasts)	Thickness: 20-70 m Area: 0.1-1.1 km ²	NE-SW elongation.
	S5	100-400	Length: 13 km Width: 11 km Area: 98 km ²	Facies 1 (debrites) and facies 2 (megaclasts)	Thickness: 70-400 m Area: 0.2-7 km ²	Vergence of folds within megaclasts, grooves & scours, onlap against levee to the N
	S6	50-130	Length: 14 km Width: 8 km Area: 80 km ²	Facies 1 (debrites) and facies 2 (megaclasts)	Thickness: 27-90 m Area: 0.04-0.5 km ²	Widening to the SW and pinch-out against megaclasts in S5.
Post-tectonic Shelf-attached	C1	50-200	Length: 40 km Width: 4-13 km Area: 300 km ²	Facies 1 (debrites) and facies 2 (megaclasts)	Thickness: 50-200 m Area: 0.06-1.6 km ²	Orientation of lateral scarps, vergence of folds and faults
	N1	50-130	Length: 45 km Width: 3-4 km Area: 244 km ² (base surf.)	Facies 1 (debrites)	None identified	Orientation of lateral scarps
	N2	20-150	Length: 35 km Width: 3-4 km Area: 220 km ² (base surf.)	Facies 1 (debrites)	None identified	Orientation of lateral scarps

Figure 5.

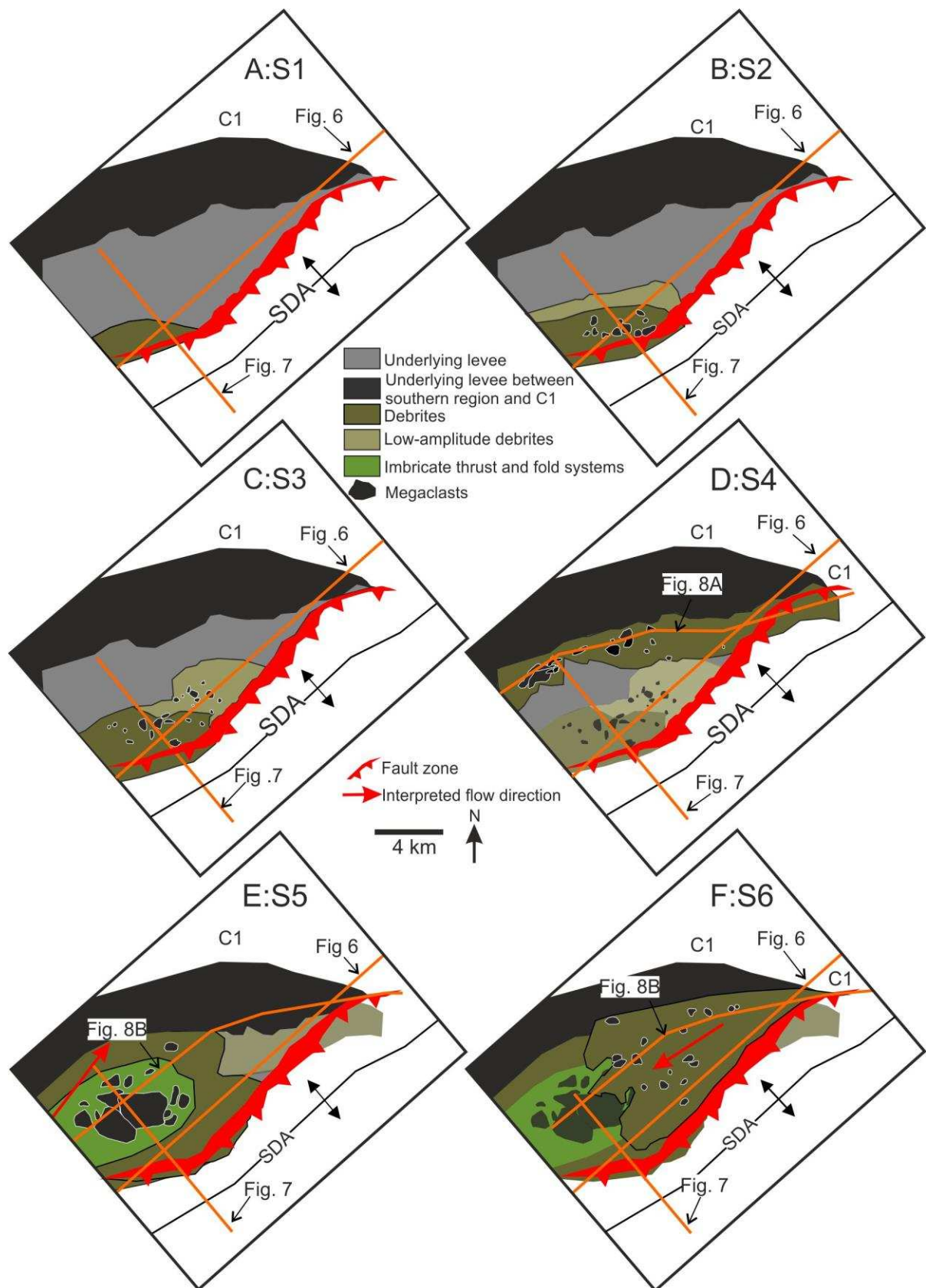


Figure 6.

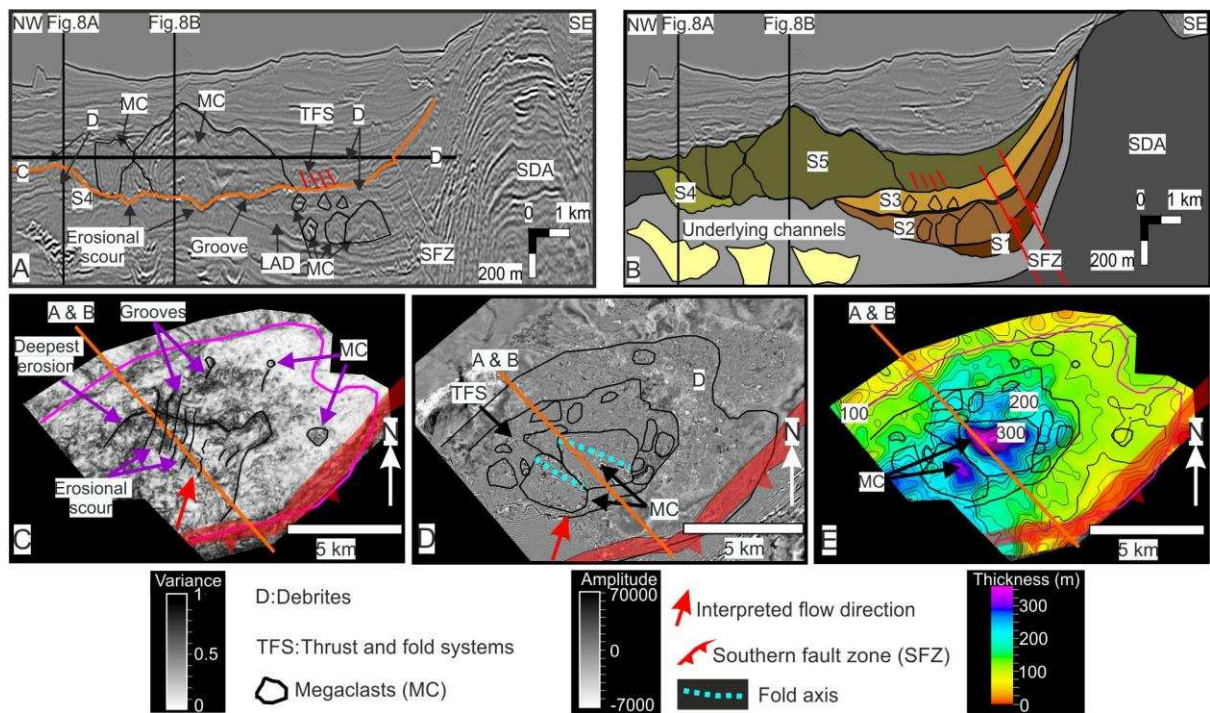


Figure 7.

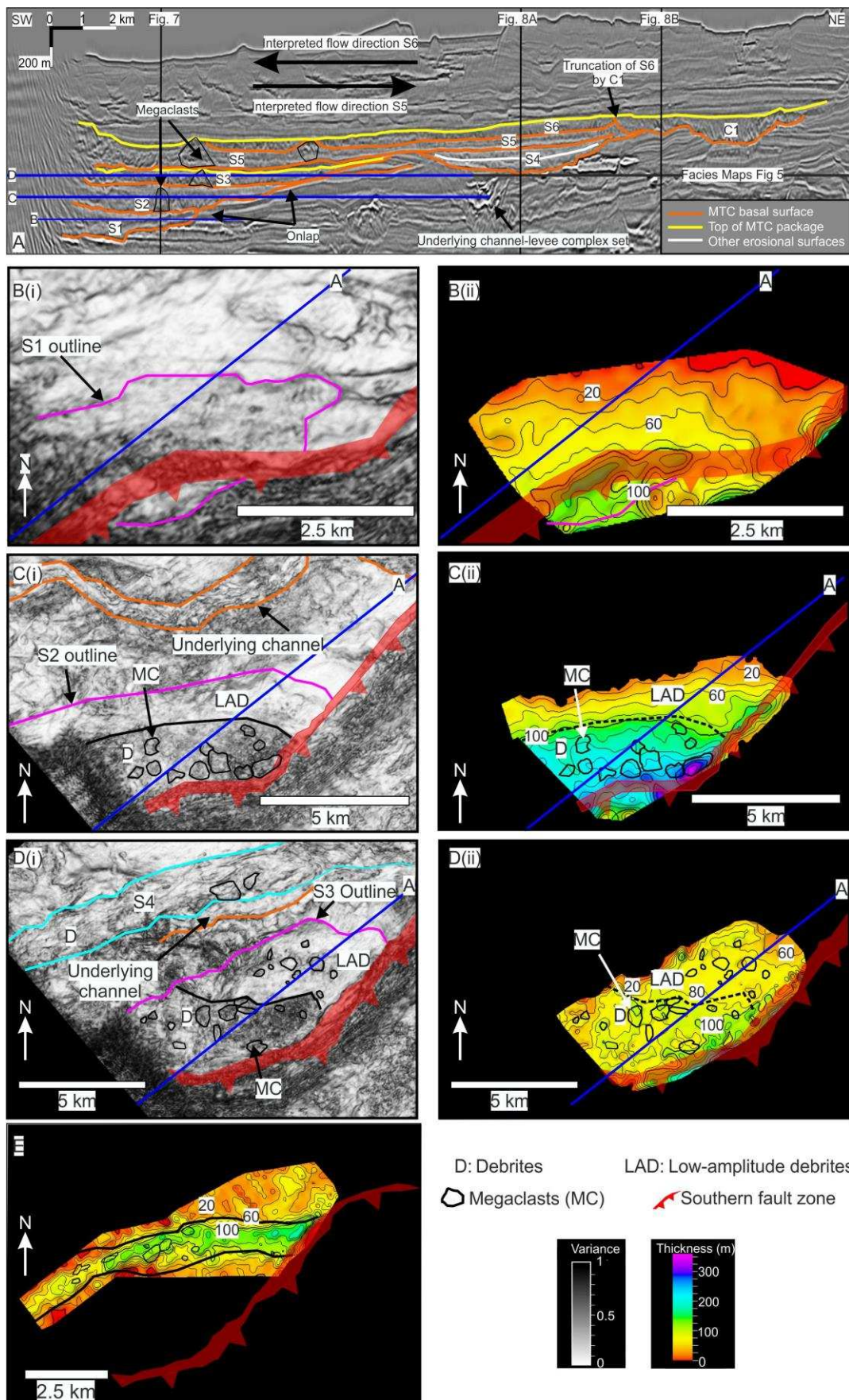


Figure 8.

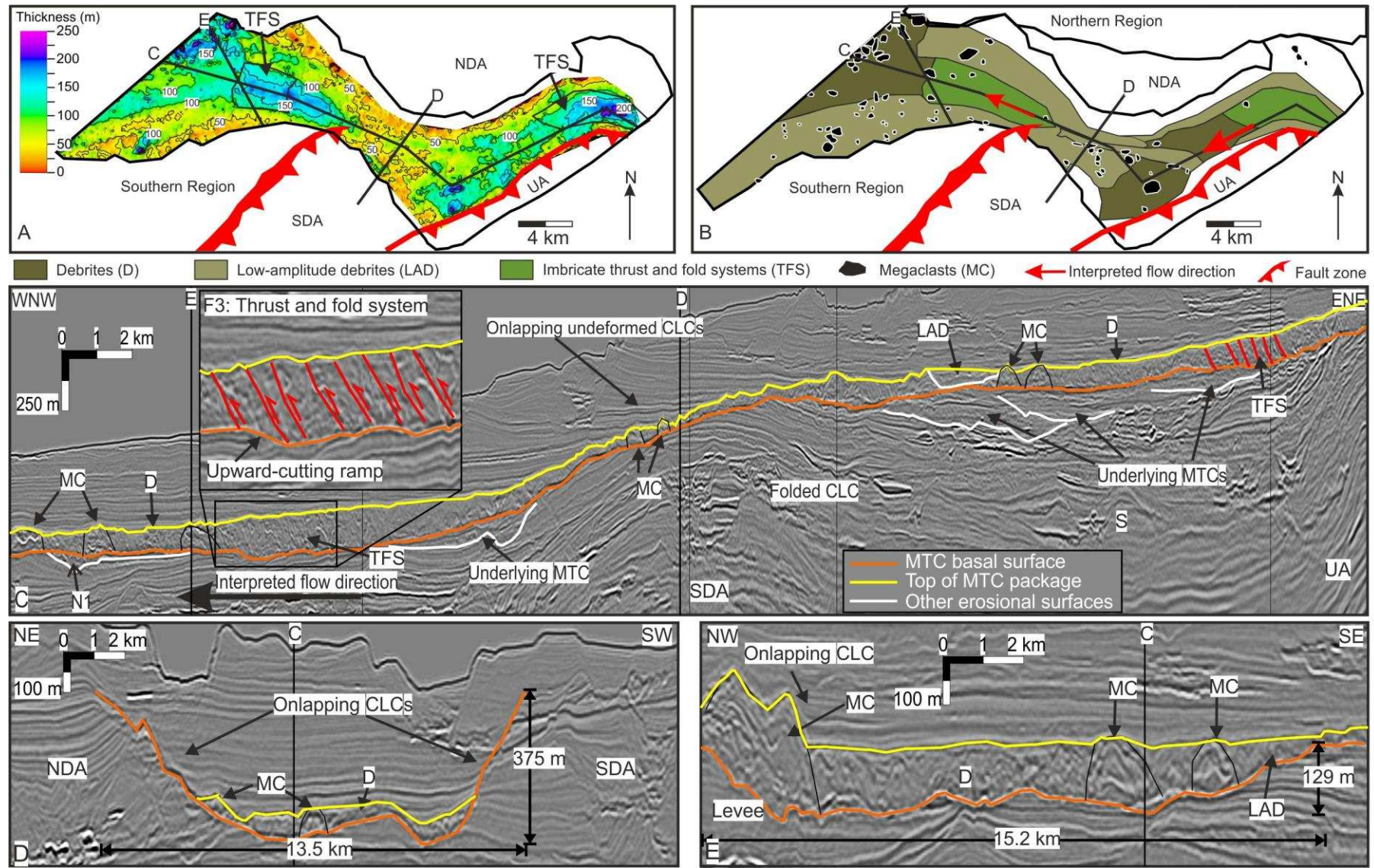


Figure 9.

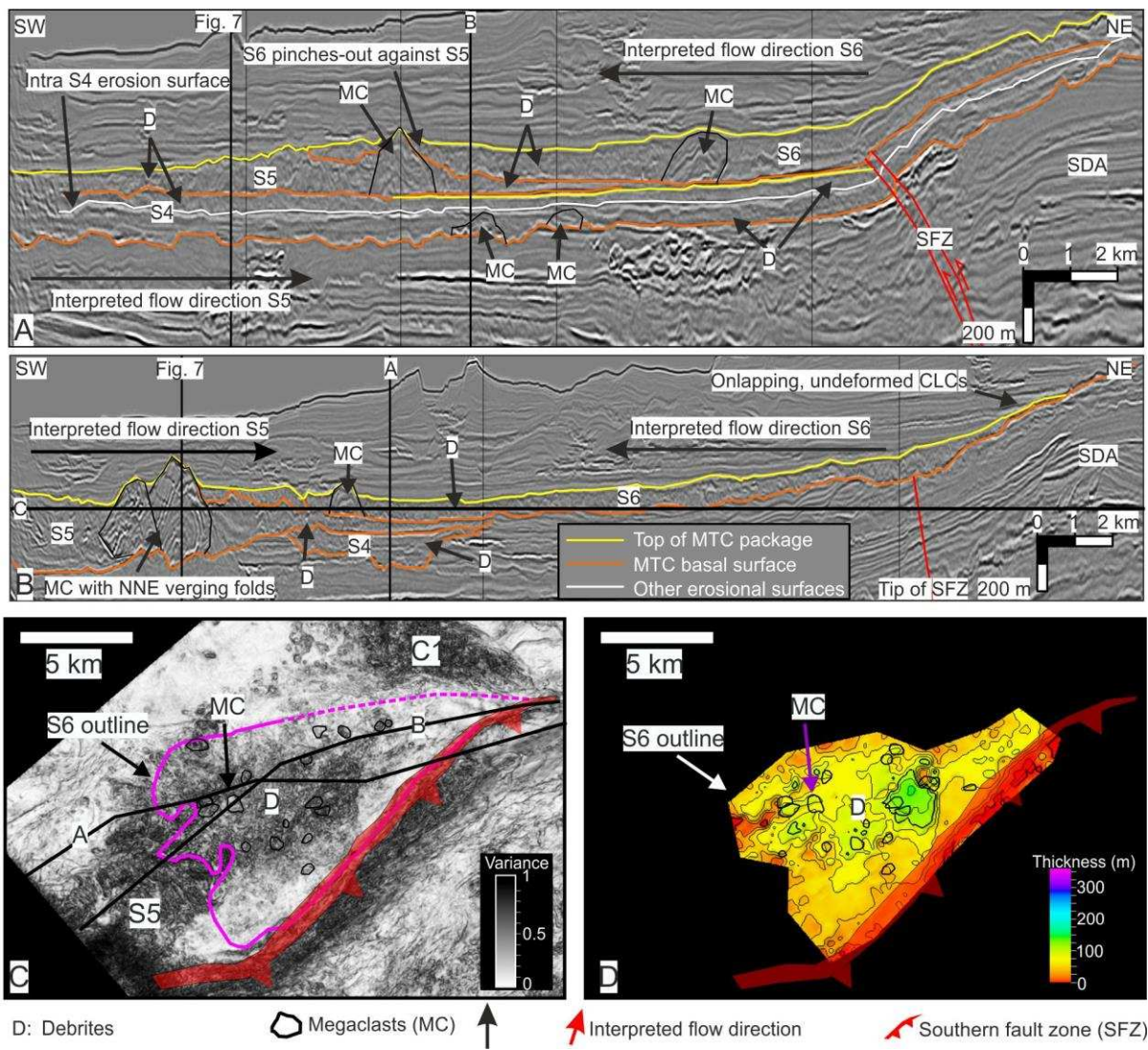


Figure 10.

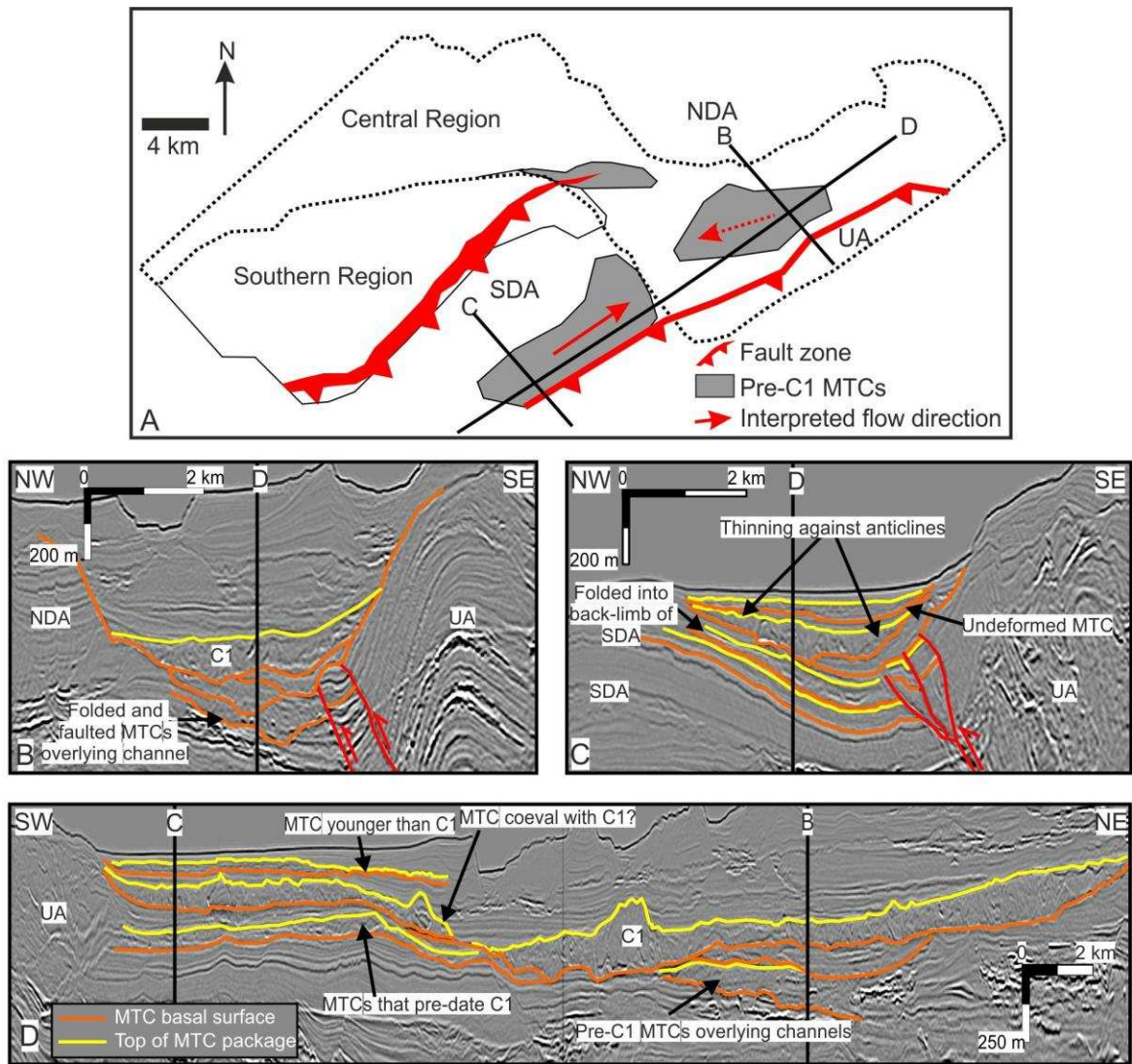


Figure 11.

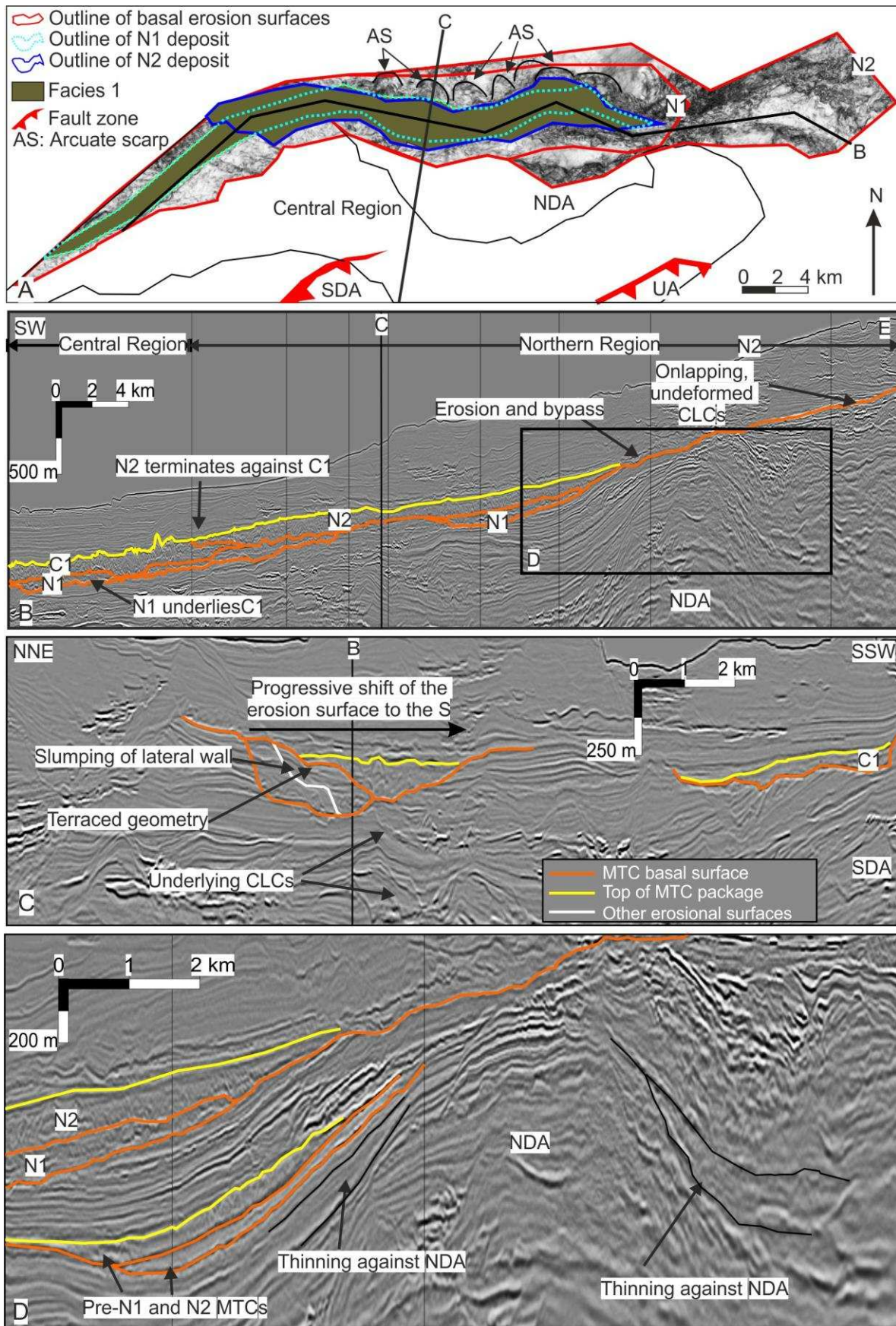


Figure 12.

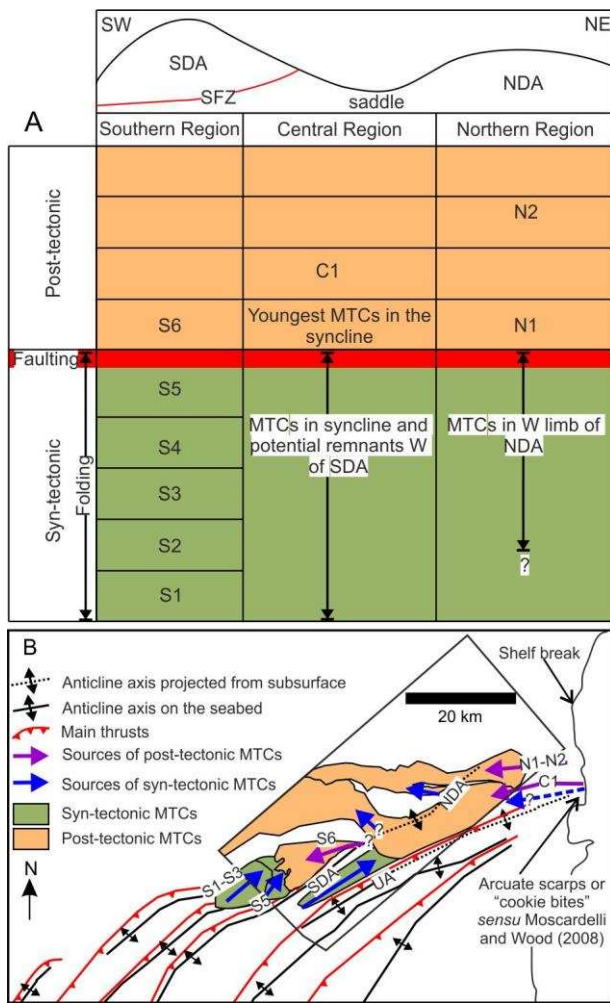


Figure 13.

